ADSORPTION OF AROMATIC MOLECULES ON RUTILE TiO_2(110) SURFACES

A THESIS SUBMITTED TO
THE GRADUATE SCHOOL OF NATURAL AND APPLIED SCIENCES
OF
MIDDLE EAST TECHNICAL UNIVERSITY

BY

MURAT MESTA

IN PARTIAL FULFILLMENT OF THE REQUIREMENTS
FOR
THE DEGREE OF MASTER OF SCIENCE
IN
PHYSICS

SEPTEMBER 2009

Approval of the thesis:

ADSORPTION OF AROMATIC MOLECULES ON RUTILE TiO_2(110) SURFACES

submitted by **MURAT MESTA** in partial fulfillment of the requirements for the degree of **Master of Science in Physics Department, Middle East Technical University** by,

Prof. Dr. Canan Özgen _____
Dean, Graduate School of **Natural and Applied Sciences**

Prof. Dr. Sinan Bilikmen _____
Head of Department, **Physics**

Prof. Dr. Şinasi Ellialtıoğlu _____
Supervisor, **Physics Department, METU**

Examining Committee Members:

Prof. Dr. Mehmet Parlak
Department of Physics, METU _____

Prof. Dr. Şinasi Ellialtıoğlu
Department of Physics, METU _____

Prof. Dr. Mehmet Çakmak
Department of Physics, Gazi University _____

Assoc. Prof. Dr. Ersen Mete
Department of Physics, Balıkesir University _____

Assist. Prof. Dr. Hande Toffoli
Department of Physics, METU _____

Date: **11.09.2009**

I hereby declare that all information in this document has been obtained and presented in accordance with academic rules and ethical conduct. I also declare that, as required by these rules and conduct, I have fully cited and referenced all material and results that are not original to this work.

Name, Last Name: MURAT MESTA

Signature :

ABSTRACT

ADSORPTION OF AROMATIC MOLECULES ON RUTILE TiO_2(110) SURFACES

Mesta, Murat
M.S., Department of Physics
Supervisor : Prof. Dr. Şinasi Ellialtıoğlu

September 2009, 49 pages

Transition metal oxides having high dielectric constants and wide band gaps find very important and interesting technological applications in surface physics. In particular, titania is the most commonly used material in heterogeneous catalysis because of its stable and flat surfaces. Having Ti cations at different charge states within the system brings about various novel electronic properties which are mainly surface related. Adsorption of catalytically important or chemically useful molecules on titania surfaces are investigated, electronic energy bands and charge densities are calculated from first principles using the density functional theory in the GGA scheme. The comparisons with the leading theories and existing experimental data are maid.

Keywords: Density functional theory, titanium dioxide, rutile, aromatic molecules, solar cell

ÖZ

RUTİL TiO_2(110) YÜZEYLERİNE AROMATİK MOLEKÜL TUTUNMASI

Mesta, Murat
Yüksek Lisans, Fizik Bölümü
Tez Yöneticisi : Prof. Dr. Şinasi Ellialtıoğlu

Eylül, 2009, 49 sayfa

Geçiş metal oksitleri, yüksek dielektrik sabitine ve geniş bant aralığına sahip olmaları nedeni ile yüzey fiziğinde çok önemli ve ilginç teknolojik uygulamalar bulmaktadır. Özellikle titanya, kararlı ve düz yüzeyleri nedeniyle heterojen katalizde en çok kullanılan malzeme olmuş durumdadır. Titanyum katyonlarının sistem içinde değişik yük-durumlarında bulunması, yüzey bağlantılı çok çeşitli ve yeni elektronik özellikleri beraberinde getirir. Bu tez çalışmasında, katalitik özellikli veya kimyasal ilginçliğe sahip moleküllerin rutil yapılı titanya yüzeyine tutunmaları incelenmiş, elektronik enerji bantları ve yük yoğunlukları ilk pensipten başlanarak GGA yordamında yoğunluk fonksiyoneli kuramı kullanılarak hesaplanmıştır. Sonuçlar, diğer öndegelen teorilerle ve güncel deneysel verilerle karşılaştırılmıştır.

Anahtar Kelimeler: Yoğunluk fonksiyonel kuramı, titanyum dioksit, rutil, aromatik moleküller, güneş pili

Anneme ve babama

ACKNOWLEDGMENTS

I would like to express my deepest gratitude to my supervisor Prof. Dr. Şinasi Ellialtıoğlu, for his endless patience and guidance all the time, to my unofficial advisor Dr. Hande Toffoli, whom I owe a lot, for her valuable assistance in theory and in many others, to Prof. Dr. Mehmet Çakmak, for his computer support without which this thesis cannot be completed, to Dr. Tuğrul Hakioğlu, for administration of the fruitful workshops at ITAP.

My special thanks go to my dear colleagues Kıvılcım Başak Vural, Engin Torun, Ceren Sibel Sayin and Ceren Tayran, for their friendship, cooperation and comments that contributed this thesis very much.

Also I would like to thank a lot to my dear physics fellows Sinan Değer, Efe Kemaneci, and Selçuk Bilmiş, for their company in this journey, to my best friends Ufuk Şenveli, Deniz Kozlu, Eralp Erman, Mete Kurşun, and Kıvanç Uyanık, for their valuable friendship and unbeatable support motivating this thesis.

This work is financially supported by TÜBİTAK, The Scientific and Technological Research Council of Turkey (Grand no: TBAG-107T560).

TABLE OF CONTENTS

CHAPTER 1

INTRODUCTION

In the early 1930s especially after the advent of quantum physics, the problem of many-body quantum mechanics had been the major topic for the physicists pioneered by Bloch, Hartree, Slater, and Dirac. They have been followed by many other scientists after solid state physics (later condensed matter) was specialized as a branch. The inevitable idea is that in order to describe the physical processes taking place in a real complex material equations of quantum mechanics, which has been proven to be the theory of the atomic scale, have to be solved. Unfortunately, except for the simplest systems, the equations are too complicated to be solved analytically. This leads scientists to solve equations numerically by tackling the problem on the computer with proper methods. Today Density Functional Theory (DFT), being one of them, has become the major tool to investigate the physical and chemical properties of condensed matter. This is due to the vast increase in computer power in addition to simplicity and computational efficiency of DFT. The theory was established by a chemist, Walter Kohn, published in a physics journal in 1964 [1] and was given the Nobel price in 1998 because of its unquestionable applicability supported by computational improvements. The importance of DFT lies under the fact that it is an ab initio method, that is, no empirical information about the system is necessary to start with and quantitative results can be reachable from first principles (a quantum mechanical description). Furthermore DFT can guide experimentalists to obtain results that are foreseen or show a path to both development and manufacturing processes of new materials (material science).

There are many implementations of DFT on the approximation of the theory (exchange–correlation) and the usage of computer power. Projected Augmented Wave (PAW) method, [2] which has been developed recently, is one of the most efficient ways to perform calculations

with its elegant framework combining the pseudopotential and augmented wave methods. The crucial point is that PAW enables one to have knowledge about not only the valence but also the core electrons which is the reason why it is called an all-electron approximation. In addition to this for the exchange–correlation, although there is no standard way to decide, in general Generalized Gradient Approximation (GGA) gives results closer to the experiments. Perdew–Burke–Enzherkof (PBE) parametrization [3] is the latest developed approximation satisfying all the conditions that has to be met by an exchange-correlation functional. In this study all of these implementations applied by the Vienna Ab-initio Simulation Package (VASP) [4] and visualizations are done with the visualization program Xcrysden [5].

This work aims to investigate titanium dioxide which is one of the most intensely studied metal oxide semiconductor from first principles. It is an inexpensive, non-toxic, and easy to manufacture semiconductor having many diverse applications especially as photoelectrochemical converter (dye solar cell or photovoltaic) [6] and photocatalyst[1] [8]. TiO_2 is the main component in the dye-sensitized solar cells as the electrode while the organic dyes are usually the most effective way to be used as the photosensitizers. In this study adsorption properties of aromatic hydrocarbons on rutile (110) surface are investigated. These molecules are the main component of the organic dyes and finding a proper way to link these with the surface has a very important place in these kinds of studies. To do so in this work two anchor groups are investigated the first being the simplest carboxylic acid, namely the formic acid and the second being a more complex adsorbate, the phosphonic acid. The purpose is to catch some trend between the number of the aromatic rings and their effects on the electronic structure when adsorbed on titania surface using these two different but well known anchors. The idea is instead of delivering a new technology, to guide related researchers who need information beyond the available experimental data.

1.1 DYE-SENSITIZED SOLAR CELL

Dye-sensitized solar cells (DSSC) are first developed by Grätzel and co-workers [6], [9]. Working principle is similar to the natural process, photosynthesis, where the dye is chlorophylls. A DSSC consists of three main parts namely substrate, photo-sensitizing dye and

[1] Also TiO_2 is used as white pigment in paints and cosmetics, as optical coating, in ceramics, as gas sensor, in electronic circuit elements like MOSFETs, in bone implantation, etc. [7]

electrolyte. The substrate is a cheap, easy to manufacture and chemically stable semiconductor whose band gap is wide absorbing only a limitted range of solar emission beyond the visible spectrum. The role of the dye is to lessen this gap allowing visible part of the spectrum be absorbable which is a necessity because the intensity of solar radiation reaching earth is the highest at this range. The important factor is that the excitations are happening through the low-energy state to high-energy state of the dye, in other words, difference between HOMO and LUMO of the dye has a crucial meaning in application. The excited electron has to be

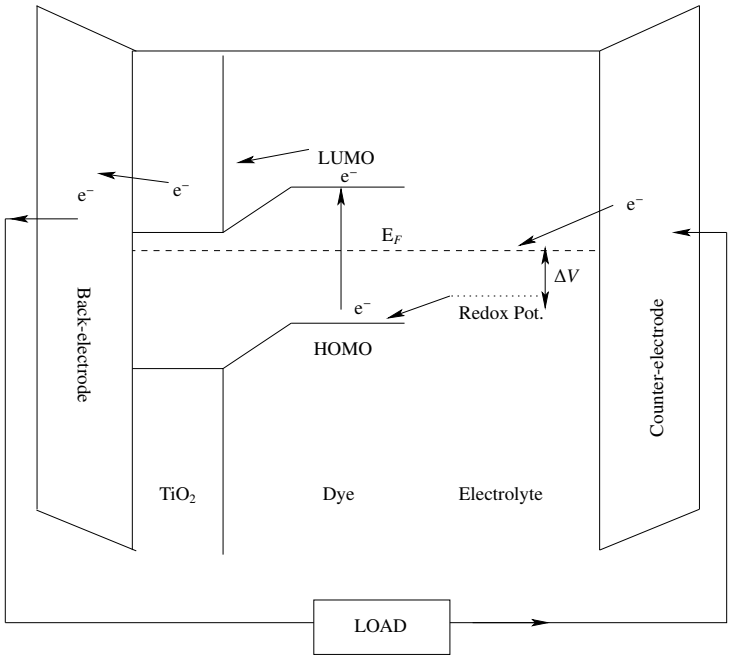

Figure 1.1: Schematic diagram of the electron transfer process in a typical DSSC

quickly injected into the conduction band of the semiconductor or else it would be recaptured by the dye itself. Thus the injection time of the excited electron has also an important place in application. The anchor group used for binding the dye to the surface function as a mediator in the surface electron transfer and affect the injection hugely. After the excited electron injected into the conduction band of the substrate, it has to return to the dye in order to prevent decomposition of the dye and to have future excitations. This is done by the back-electrode placed in the semiconductor and it is the major difference between a DSSC and a conventional solar cell because the charge transfer is separated from the absorption process. In fact the lost electron of the dye is covered by the electrolyte much before the excited one reaches the counter electrode which at the end supplies required electron to the electrolyte (reduction). Schematic diagram of a DSSC is represented in 1.1. The process starts from the excitation of

the electron in the dye from dye-LUMO to the HOMO which oxidizes the dye. The electron moves on its way to the conduction band of substrate (TiO_2) while the electrolyte supplies the lost electron of the dye ending up with a oxidized state. The photoelectron passes to the external load through the back-contact and continue to the counter-electrode where reduction of the electrolyte is provided returning the system to its groundstate for further excitations. The maximum output voltage is the difference between Fermi energy of the system and the redox potential of the electrolyte.

CHAPTER 2

MANY-BODY QUANTUM MECHANICS

For any condensed matter system a description of the physical phenomena comprised by electrons and nuclei can be obtained only by solving the equations of quantum mechanics. However electrons and nuclei are mutually interacting because of their charges. If the treatment is non-relativistic, one has to solve the Schrödinger equation constructed with the Hamiltonian describing the interactions and at the end obtain a wave function depending on both electronic and nuclear spatial coordinates. Considering this the Hamiltonian can be written as[1],

$$\begin{aligned} H &= \sum_{i=1}^{N} -\frac{1}{2}\nabla_i^2 + \sum_{k=1}^{M} -\frac{1}{2M_k}\nabla_k^2 + \sum_{i=1}^{N}\sum_{j>i}^{N} \frac{1}{\mid \mathbf{r}_i - \mathbf{r}_j \mid} - \sum_{i=1}^{N}\sum_{k=1}^{M} \frac{Z_k}{\mid \mathbf{r}_i - \mathbf{R}_k \mid} \\ &+ \sum_{k=1}^{M}\sum_{l=1}^{M} \frac{Z_k Z_l}{\mid \mathbf{R}_k - \mathbf{R}_l \mid} \end{aligned} \tag{2.1}$$

and the eigenvalue equation reads

$$H\psi(\mathbf{r}, \mathbf{R}) = E\psi(\mathbf{r}, \mathbf{R}) \tag{2.2}$$

where the first two terms in the Hamiltonian are the kinetic energies of electrons and ions and the rest are electron–electron, electron–nuclei and nuclei–nuclei interactions with $\mathbf{r}$ representing all electronic coordinates and $\mathbf{R}$ all nuclear coordinates. If there are N electrons and M ions obtaining such an exact wave function is not possible. The first simplification is the so called Born–Oppenheimer approximation [10] which allows to separate the wave function into electronic and nuclear parts owing to the large mass difference between electrons and ions ($10^{-5} \leq m/M \leq 10^{-3}$) (see Appendix A). Therefore the kinetic energy of nuclei T_n vanishes. Moreover for a frozen lattice nuclear–nuclear repulsion is a constant bringing just a phase factor to the wavefunction (in time dependent case) leaving all expectation values

[1] Atomic units are used, i.e, $m = e = \hbar = 1$, unit of length is Bohr and unit of energy is Hartree

unchanged. Eliminating all of these the Hamiltonian now becomes

$$H_e = \sum_{i=1}^{N} -\frac{1}{2}\nabla_i^2 + \sum_{i=1}^{N}\sum_{j>i}^{N} \frac{1}{\mid \mathbf{r}_i - \mathbf{r}_j \mid} - \sum_{i=1}^{N}\sum_{k=1}^{M} \frac{Z_k}{\mid \mathbf{r}_i - \mathbf{R}_k \mid}. \tag{2.3}$$

Thus the problem is reduced to an electronic problem where N electrons are in a static external potential created by the nuclei. The positions of nuclei are now just parameters where for each set of which the electronic Schrödinger equation has to be solved with the appropriate external potential,

$$H = T + U + V_{\text{ext}}$$

$$H\psi(\mathbf{r}_1, \mathbf{r}_2, ..., \mathbf{r}_N) = E\psi(\mathbf{r}_1, \mathbf{r}_2, ..., \mathbf{r}_N). \tag{2.4}$$

Solution of (2.4) is the fundamental issue in the theory of electronic structure and DFT is a feasible way to attack this problem. Before going into more details about DFT it is better to introduce some preliminaries which are used largely in DFT calculations.

2.1 Variational Principle and Lagrange Multipliers

The Schrödinger equation with the Hamiltonian in (2.1) can be solved exactly in very few cases due to the interaction terms. One way to obtain an approximate solution is the variational principle where for most of the case approximation is good enough to reproduce experimental conclusions. The method simply proposes that ground state energy obtained from any trial wavefunction is always greater or equal to the exact ground state energy. The proof [11] is as follows.

Exact eigenstates[2] $\mid \psi_n \rangle$ of H form a complete set and any approximate wavefunction $\mid \phi \rangle$ can be expanded in terms of such basis functions

$$\mid \phi \rangle = \sum_n c_n \mid \psi_n \rangle, \qquad H \mid \psi_n \rangle = E_n \mid \psi_n \rangle.$$

Assuming ψ_n's are orthonormal

$$\langle \phi \mid \phi \rangle = \sum_m \sum_n c_m^* c_n \langle \psi_m \mid \psi_n \rangle = \sum_n \mid c_n \mid^2 .$$

Similarly

$$\langle \phi \mid H \mid \phi \rangle = \sum_m \sum_n c_m^* c_n \langle \psi_m \mid H \mid \psi_n \rangle = \sum_n E_n \mid c_n \mid^2 .$$

[2] In general exact eigenfunctions of H are not known, thus the trial wave function is expanded in terms of other known basis functions such as Gaussians or plane waves.

Noting $E_0 \leq E_1 \leq E_2 \ldots$

$$\sum_n E_0 \mid c_n \mid^2 \leq \sum_n E_n \mid c_n \mid^2$$

and

$$E = \frac{\langle \phi \mid H \mid \phi \rangle}{\langle \phi \mid \phi \rangle} = \frac{\sum_n E_n \mid c_n \mid^2}{\sum_n \mid c_n \mid^2} \geq \frac{\sum_n E_0 \mid c_n \mid^2}{\sum_n \mid c_n \mid^2}.$$

Therefore

$$E_0 \leq \langle \phi \mid H \mid \phi \rangle. \tag{2.5}$$

Equation (2.5) indicates that for any trial wavefunction, the expectation value of H is an upper bound to the ground state energy[3] and by choosing a clever trial function it can be accurately guessed. The best way to guess an accurate trial function is to introduce a large number of adjustable parameters. Minimization over these parameters will yield the lowest possible eigenvalue (λ) and thus a better guess to the ground state.

In order to satisfy wavefunction normalization (constraint) the variational problem can be reformulated using Lagrange's method of undetermined multipliers [12] which is largely used in classical mechanics to solve constrainted variational problems. Define the functional

$$K[\phi] = \langle \phi \mid H \mid \phi \rangle - \lambda(\langle \phi \mid \phi \rangle - 1).$$

The coefficient λ is called Lagrange multiplier and it is clear that minimization over it guaranties the normalization. Although the coefficient λ seems arbitrary, it corresponds to a physically meaningful quantity. In order to see this consider minimizing the functional $K[\phi]$ with respect to expansion coefficients c_n. First writting K explicitly (a more general case where basis functions $\mid \psi_n \rangle$ may not be orthonormal)

$$\begin{aligned} K &= \sum_m \sum_n c_m^* c_n \langle \psi_m \mid H \mid \psi_n \rangle - \lambda \left(\sum_m \sum_n c_m^* c_n \langle \psi_m \mid \psi_n \rangle - 1 \right) \\ &= \sum_{m,n} c_m^* c_n H_{mn} - \lambda \left(\sum_{m,n} c_m^* c_n S_{mn} - 1 \right) \end{aligned}$$

where $\mathbf{S}$ is the overlap matrix containing all the inner products $\langle \psi_m \mid \psi_n \rangle$. Now, minimizing gives

$$\begin{aligned} \frac{\partial K}{\partial c_k} = \frac{\partial K}{\partial c_k^*} &= 0 \\ &= \sum_n H_{kn} c_n - \lambda \sum_n S_{kn} c_n = 0. \end{aligned} \tag{2.6}$$

[3] Energy is now a *functional* of the approximate wavefunction $\phi(\mathbf{r})$

This can be written in matrix form as

$$\mathbf{H} \cdot \mathbf{C} = \lambda \mathbf{S} \cdot \mathbf{C} \tag{2.7}$$

which is a generalized eigenvalue equation and if the basis is orthonormal the matrix $\mathbf{S}$ is just the identity matrix. Multiplying both sides of equation (2.6) with c_k^* and summing over the index k (or multiplying the matrix equation by $\mathbf{C}^\dagger$ from left) gives

$$\lambda = \frac{\sum_{k,n} c_k^* c_n \langle \psi_k \mid H \mid \psi_n \rangle}{\sum_{k,n} c_k^* c_n \langle \psi_k \mid \psi_n \rangle} = \langle E \rangle. \tag{2.8}$$

Equation (2.8) shows that the eigenvalues of (2.7) are not arbitrary numbers but they are physically meaningfull energy eigenvalues of the Hamiltonian H.

2.2 The Hellmann–Feynman Theorem

This theorem first published by the German physicist Hans Hellmann. Feynman's work, which is an undergraduate thesis, published four years later independent from the former. In this section the theorem is summarized following Feynman's method [13] which is easier to follow owing to usual Feynman style.

In order to calculate the force on a nucleus one should calculate the energy of the system (all electrons and nuclei) for several different nuclear positions by the variational method or other perturbation scheme. Then the slope of the energy *vs.* position plot will give the desired force. However this calculation is cumbersome since energy calculation needs to be done for at least two different configurations. Feynman suggested only one configuration, the one in question, need have its wavefunctions computed to obtain the force.

Let λ be any one of the parameters specifying nuclear positions, for example x component of the position of one of the nuclei. Requiring the system is in a steady state of energy E the corresponding force f_λ can be calculated as follows;

$$f_\lambda = -\frac{\partial E}{\partial \lambda} = -\frac{\partial}{\partial \lambda} \langle \psi \mid H \mid \psi \rangle = -\left\langle \frac{\partial \psi}{\partial \lambda} \mid H \mid \psi \right\rangle - \left\langle \psi \mid \frac{\partial H}{\partial \lambda} \mid \psi \right\rangle - \left\langle \psi \mid H \mid \frac{\partial \psi}{\partial \lambda} \right\rangle.$$

Since H is a self-adjoint operator

$$\left\langle \psi \mid H \mid \frac{\partial \psi}{\partial \lambda} \right\rangle = \left\langle \frac{\partial \psi}{\partial \lambda} \mid H \mid \psi \right\rangle^*$$

and $H \mid \psi\rangle = E \mid \psi\rangle$, $\langle\psi \mid H^{\dagger} = \langle\psi \mid E$ with $\langle\psi \mid \psi\rangle = 1$ so

$$f_{\lambda} = -\left\langle \psi \mid \frac{\partial H}{\partial \lambda} \mid \psi \right\rangle - E\frac{\partial}{\partial \lambda}\langle\psi \mid \psi\rangle$$

$$f_{\lambda} = -\left\langle \psi \mid \frac{\partial H}{\partial \lambda} \mid \psi \right\rangle. \tag{2.9}$$

Calculation of $\langle\frac{\partial H}{\partial \lambda}\rangle$ is not too different from $\langle H\rangle$ and in practice it is easier to calculate the force using this expectation value rather than an approximation of the derivative by using the energy differences. In fact the Hamiltonian H depends on the nuclear positions explicitly and in the frame work of Born-Oppenheimer approximation these are just parameters, thus the theorem becomes an electrostatic theorem. The force on the nucleus α along the nuclear position λ is determined by

$$f_{\lambda}^{\alpha} = \left\langle -\frac{\partial}{\partial \lambda_{\alpha}} \left(\sum_{l=1}^{M} \frac{Z_{\alpha} Z_{l}}{\mid \mathbf{R}_{\alpha} - \mathbf{R}_{l} \mid} - \sum_{i=1}^{N} \frac{Z_{\alpha}}{\mid \mathbf{r}_{i} - \mathbf{R}_{\alpha} \mid} \right) \right\rangle \tag{2.10}$$

which is the change in nuclear-nuclear repulsion and electron-ion attraction with respect to the ion positions. Since both of the potentials are known in a DFT calculation, obtaining forces on ions is not cumbersome. This can be trivially extended for any expectation value of a Hermitian operator.

CHAPTER 3

DENSITY FUNCTIONAL THEORY

Shortly after Schrödinger's equation for the electronic wavefunction had been introduced there a common belief among physicists that is well understood from P.A.M. Dirac famous saying was;

> The fundamental laws necessary for the mathematical treatment of a large part of physics and the whole of chemistry are thus completely known, and the difficulty lies only in the fact that application of these laws leads to equations that are too complex to be solved.

This is still valid if one tries to solve the Schrödinger equation written for a many electron system. Density Functional Theory (DFT) comes in as an alternative approach to the theory of electronic structure where the electronic density is the major tool to calculate all the physical quantities in question. Rather than the many-body wave function itself, which is constructed from single-particle orbitals as Slater determinants (a demanding process), the electronic density is much more computationally efficient because it is a three dimensional real space function (function of position vector). This makes DFT a versatile tool and due to this it has turned out to be the main technique for the study of matter at the nanometric scale for the last decade.

3.1 Thomas–Fermi Model

The idea of constructing the total energy in terms of the electronic density was originally developed independently by Thomas in 1927 [14] and Fermi in 1928 [15]. In the original work the purpose was stated as calculating observables of atoms (like effective electric field

inside the atom) without using any experimental fitting, thus to know effective electric field inside the atom. There is a statistical consideration with the key assumption that electrons of a nuclei are uniformly distributed over the phase space where for each electron a cube of volume h^3 is separated and the potential is determined by this distribution of electrons which is a function of position vector only. As seen clearly there is no correlation between electrons and they are just uniformly distributed over the space only considering a statistical weight. Therefore this approximation may be valid for large densities or interior of heavy atoms where correlation effects are low and the electrons form a Fermi sphere (fermionic properties are more important than the correlation).

The derivation [16] simply follows from statistical properties of the homogeneous electron gas and a local approximation to inhomogeneous system. For a uniform free-electron gas, volume of occupied phase space is simply $4/3\pi p_F^3 V$ where V is the volume in real space and p_F is the largest momentum and the states having greater momenta are unfilled. Owing to the uncertainty principle each state corresponds to a cell of volume h^3 in phase space and for the ground state each cell can be occupied by two electrons having opposite spins. Thus the number of electrons and the density can be written as

$$N = 2\frac{4\pi p_F^3}{3h^3}V, \qquad n = \frac{8\pi}{3h^3}p_F^3.$$

This can be applied to an atomic system stating that $\mathbf{p}_F$ is a function of the position vector as well as the density. Next step is to denote the probability P of an electron at the postion $\mathbf{r}$ having a momentum of magnitude between p and $p + dp$ as

$$P\,dp = \frac{4\pi p^2}{4/3\pi p_F(\mathbf{r})}dp, \qquad p < p_F(\mathbf{r}).$$

Kinetic energy of the system is a statistical integration and can be written as

$$T = \int d\mathbf{r}\, n(\mathbf{r}) \int_0^{p_F(\mathbf{r})} dp\, \frac{p^2}{2m}\frac{3p^2}{p_F^3(\mathbf{r})}.$$

Writing p_F in terms of the density, the kinetic energy reduces to

$$T_{\mathrm{TF}}[n] = C_F \int n^{5/3}(\mathbf{r})\, d\mathbf{r}, \qquad C_F = \frac{3h^2}{10m}\left(\frac{3}{8\pi}\right)^{2/3}. \tag{3.1}$$

Also the total energy can be written as

$$E_{\mathrm{TF}}[n] = C_F \int n^{5/3}(\mathbf{r})\, d\mathbf{r} + Z\int \frac{n(\mathbf{r})}{\mathbf{r}}\, d\mathbf{r} + \frac{1}{2}\iint \frac{n(\mathbf{r_1})n(\mathbf{r_2})}{|\,\mathbf{r_1}-\mathbf{r_2}\,|}\, d\mathbf{r_1}d\mathbf{r_2} \tag{3.2}$$

where the interactions are treated as classical Coulombic interactions and quantum mechanical contributions are ignored (Hartree-type potential). Exchange can be included by a further assumption that momenta and coordinates of electrons commute reducing the problem to a classical one but keeping two electrons in the volume $2\pi h$ [17] and correlations can also be approximated by a function of space only,for example [18]. However none of these corrections provide higher accuracy than previous approximations like Hartree-Fock have been constructed. Also the kinetic energy (3.1) is constructed with a density not including correlations and since the kinetic energy is the dominating term for a Coulombic system, Thomas-Fermi approximation does not give accurate results for quantitative treatments if the correlations are important. One last note is that although the energy is written in terms of density, Thomas-Fermi approximation does not give any proof to that energy can always be written as a functional of density.

3.2 The Hohenberg–Kohn Theorems

The formal starting point of DFT is the two simple theorems published by Hohenberg and Kohn in 1964 [1]. The idea is to prove that ground state wavefunction of a many-body system can always be linked to the corresponding ground state charge density. At first glance writing down a function of N variables (coordinates of N electrons) using charge density, which is a function of one variable (position vector), seems impossible but charge density is not an arbitrary function. It includes all the information which can be extracted from the ground state wave function. All of these need a proof showing that the density is the basic variable.

Hohenberg–Kohn Theorem I

> For a given N-particle electronic density $n(\mathbf{r})$ of a non-degenerate ground state corresponding to an external potential V_{ext}, the density determines this potential uniquely.

Proof. Assume that two different potentials $V_{\text{ext}}(\mathbf{r})$ and $V'_{\text{ext}}(\mathbf{r})$ with ground states ψ and ψ' are determined by the same density. If $V_{\text{ext}}(\mathbf{r}) - V'_{\text{ext}}(\mathbf{r}) \neq \text{const}$ then clearly $\psi \neq \psi'$. Ground state energies corresponding to each Hamiltonian can be written as $E = \langle \psi \mid H \mid \psi \rangle$ and

$E' = \langle \psi' \mid H' \mid \psi' \rangle$, then by the variational principle

$$E < \langle \psi' \mid H \mid \psi' \rangle \tag{3.3}$$

$$E' < \langle \psi \mid H' \mid \psi \rangle. \tag{3.4}$$

Since H and H' differ only in external potentials one can write

$$\begin{aligned} \langle \psi' \mid H \mid \psi' \rangle &= \langle \psi' \mid H' \mid \psi' \rangle - \langle \psi' \mid (V_{\text{ext}} - V'_{\text{ext}}) \mid \psi' \rangle \\ \langle \psi \mid H' \mid \psi \rangle &= \langle \psi \mid H \mid \psi \rangle + \langle \psi \mid (V_{\text{ext}} - V'_{\text{ext}}) \mid \psi \rangle. \end{aligned}$$

Using above equalities and noting $\langle \psi' \mid (V_{\text{ext}} - V'_{\text{ext}}) \mid \psi' \rangle = \int (V_{\text{ext}} - V'_{\text{ext}}) n(\mathbf{r}) d(r)$, (3.3) and (3.4) can be written as

$$\begin{aligned} E &< E' + \int (V_{\text{ext}} - V'_{\text{ext}}) n(\mathbf{r})\, d\mathbf{r} \\ E' &< E - \int (V_{\text{ext}} - V'_{\text{ext}}) n(\mathbf{r})\, d\mathbf{r}. \end{aligned}$$

Summing side by side leads to the contradiction

$$E + E' < E' + E \tag{3.5}$$

which proves the initial assertion by *reductio ad absurdum* (proof by contradiction).

As a corollary one can assert that $V_{\text{ext}}(\mathbf{r})$ is a unique functional of $n(\mathbf{r})$ and since H is classified by $V_{\text{ext}}(\mathbf{r})$, $n(\mathbf{r})$ also determines the ground state wave function. In other words, ground state is also a unique functional of $n(\mathbf{r})$ so be the expectation value of any operator calculated with ψ. Total ground state energy thus can be written in functional form as

$$\begin{aligned} E[n] &= \langle \psi[n] \mid H \mid \psi[n] \rangle = \langle \psi[n] \mid T + U \mid \psi[n] \rangle + \int V_{\text{ext}}(\mathbf{r}) n(\mathbf{r}) d\mathbf{r} \\ &= F[n] + \int V_{\text{ext}}(\mathbf{r}) n(\mathbf{r}) d\mathbf{r} \end{aligned} \tag{3.6}$$

where $F[n]$ is a universal functional which is the same for all N-electron interacting systems with density $n(\mathbf{r})$.

Hohenberg–Kohn Theorem II

> Minimization with respect to density defines an upper bound to the exact ground state, i.e $E_0 \leq E[n'(\mathbf{r})]$.

Proof. Using the first theorem a given density $n'(\mathbf{r})$ determines its own potential therefore the ground state wave function ψ'. If this wave function is used as a trial wave function to calculate expectation value of the energy then by variational principle

$$\begin{aligned} E_0 \leq \langle \psi' \mid H \mid \psi' \rangle &= \langle \psi'[n'] \mid T + U \mid \psi'[n'] \rangle + \langle \psi'[n'] \mid V_{\text{ext}} \mid \psi'[n] \rangle \\ &= F[n'] + \int V_{\text{ext}}(\mathbf{r}) n'(\mathbf{r}) d\mathbf{r} = E[n'(\mathbf{r})]. \end{aligned}$$

Second theorem is a restatement of the variational principle and this time variation is a functional one with the restriction $\int n(\mathbf{r}) d\mathbf{r} = N$.

3.3 The Kohn–Sham Equations

Density functional theory was constructed by Hohenberg and Kohn through two simple theorems but they are insufficient by themselves if one wants to consider DFT as a practical scheme. This was done by Kohn and Sham [19] who succeeded in mapping the problem of interacting electrons onto an auxiliary system of non-interacting electrons. The idea is that there always exists a non-interacting system in an external potential whose density $n_s(\mathbf{r})$ is equal to the density of interacting system $n(\mathbf{r})$. The problem is now a Hartree–Fock like problem and a set of equations have to be solved *self-consistently*. The important point is that this time exchange and correlations are included through a functional of density where application of different kinds of approximation is possible.

The auxiliary non-interacting system can be described by the Hamiltonian

$$H_s = T + V_s$$

and energy

$$E_s[n] = T_s[n] + \int d\mathbf{r} V_s(\mathbf{r}) n(\mathbf{r}). \tag{3.7}$$

Since there are no interactions between electrons the density of the system is simply the sum of individual densities

$$n_s(\mathbf{r}) = \sum_{i=1}^{N} \mid \phi_i(\mathbf{r}) \mid^2 \tag{3.8}$$

where $\phi_i(\mathbf{r})$ are called Kohn–Sham orbitals and they are solutions to one-particle Schrödinger

equation with the potential $V_s(\mathbf{r})$

$$\left(-\frac{1}{2}\nabla^2 + V_s(\mathbf{r})\right)\phi_i(\mathbf{r}) = \epsilon_i\phi_i(\mathbf{r}). \tag{3.9}$$

The question, being at the heart of the formalism is what is the form of $V_s(\mathbf{r})$ so that $n_s(\mathbf{r}) = n(\mathbf{r})$. It is possible to write the energy functional as

$$E[n] = \int d\mathbf{r} V_{\text{ext}}(\mathbf{r})n(\mathbf{r}) + \frac{1}{2}\iint d\mathbf{r}d\mathbf{r}'\frac{n(\mathbf{r})n(\mathbf{r}')}{\mid \mathbf{r}-\mathbf{r}' \mid} + T_s[n] + E_{xc}[n]. \tag{3.10}$$

Here $T_s[n]$ is the kinetic energy of non-interacting electrons with density $n_s(\mathbf{r})$ and $E_{xc}[n]$ is the exchange–correlation energy of interacting system[1]. Approximation to the exchange–correlation functional done by Kohn and Sham is now known as the local density approximation (see Subsection 3.4.1 for detailed discussion) but for a general treatment considering it as in functional form

$$E_{xc}[n] = T[n] - T_s[n] + U[n] - \frac{1}{2}\iint d\mathbf{r}d\mathbf{r}'\frac{n(\mathbf{r})n(\mathbf{r}')}{\mid \mathbf{r}-\mathbf{r}' \mid}$$

and define

$$V_{xc}(\mathbf{r}) = \frac{\delta E_{xc}[n]}{\delta n(\mathbf{r})}. \tag{3.11}$$

Minimization of the energy functional gives

$$\frac{\delta E[n]}{\delta n(\mathbf{r})} = \frac{\delta T_s[n]}{\delta n(\mathbf{r})} + \int d\mathbf{r}'\frac{n(\mathbf{r}')}{\mid \mathbf{r}-\mathbf{r}' \mid} + V_{\text{ext}}(\mathbf{r}) + V_{xc}(\mathbf{r}) = 0. \tag{3.12}$$

Also from minimization of (3.7)

$$\frac{\delta E_s[n]}{\delta n(\mathbf{r})} = \frac{\delta T_s[n]}{\delta n(\mathbf{r})} + V_s(\mathbf{r}) = 0.$$

Combining this with (3.12) gives $V_s(\mathbf{r})$ as

$$V_s(\mathbf{r}) = V_{\text{ext}}(\mathbf{r}) + \int d\mathbf{r}'\frac{n(\mathbf{r}')}{\mid \mathbf{r}-\mathbf{r}' \mid} + V_{xc}(\mathbf{r}). \tag{3.13}$$

Note again that there no approximation has been done yet and $V_{xc}(\mathbf{r})$ has to be approximated to get solutions for interacting Coulombic system. The solutions have to be self-consistant, i.e. for a trial density, $V_s(\mathbf{r})$ is calculated from (3.13) then with this potential one-particle Schrödinger equation (3.9) is solved to get Kohn–Sham orbitals $\phi_i(\mathbf{r})$ which gives the new density from relation (3.8) and this iterative cycle continues until the difference between calculated densities are small enough. Figuratively

$$n(\mathbf{r}) \rightarrow V_s(\mathbf{r}) \rightarrow \text{ one-particle Sch.} \rightarrow \phi_i(\mathbf{r}) \rightarrow n_s(\mathbf{r}) \rightarrow \text{if } n_s(\mathbf{r}) \approx n(\mathbf{r}) \text{ stop.}$$

[1] Till here nothing is approximated but clearly to get a solution to the interacting problem $E_{xc}[n]$ has to be approximated. In fact one can say that unlike Hartree-Fock theory which is built as an approximation and solved exactly, DFT is an exact theory but the solution is an approximation due to $E_{xc}[n]$

3.4 Exchange and Correlation Functionals

In order for a DFT calculation to model a real system and to calculate the potential (3.11), an accurate and workable approximation to exchange–correlation functional is necessary. In fact being one of the greatest advantage of DFT, the formalism properly isolates the analytically unsolvable part, the exchange–correlation. Today construction of more accurate functional is an active research field especially for strongly correlated systems. Nevertheless, unlike other wavefunction based methods, in DFT there is no standart way to improve these approximations, that is, DFT always needs a comparison with a more accurate method (such as Configuration Interaction or Møller–Plesset(n)) to check the validity of the approximation. This is the greatest disadvantage of DFT preventing it to be a *full* ab initio method but rather a parametrization.

3.4.1 The Local Density Approximation

The first approximation to be suggested was the Local Density Approximation (LDA) [19]. As its name suggests LDA ignores non-local aspects of $V_{xc}(\mathbf{r})$ whose correct form has to be obtained from both the density at point $\mathbf{r}$ (local one) and the density at other points $\mathbf{r}'$ (non-local) which generally cannot be constructed. The idea is to have a computationally convenient approximation to model the exchange–correlation of the system by using the properties of homogeneous electron gas,

$$E_{xc}^{\mathrm{LDA}}[n] = \int d\mathbf{r}\, n(\mathbf{r})\epsilon_{xc}(\mathbf{r}, n(\mathbf{r})). \tag{3.14}$$

Here $\epsilon_{xc}[n]$ is the exchange–correlation energy per particle of a uniform electron gas with the same density of the system $n(\mathbf{r})$ [2]. This integral is like a weighted average of ϵ_{xc} where weighting function is $n(\mathbf{r})$. The homogeneous electron gas is widely studied in literature and its properties are well known which can also be implemented into LDA. One can start by separating ϵ_{xc} into exchange and correlation,

$$\epsilon_{xc}(n) = \epsilon_x(n) + \epsilon_c(n)$$

[2] $\epsilon_{xc}(n)$ is not a functional of $n(\mathbf{r})$ because whole function is not mapped to a number instead for each value of position $\mathbf{r}$ $\epsilon_{xc}(\mathbf{r}, n(\mathbf{r}))$ is calculated using $n(\mathbf{r})$ which is a number for each value of $\mathbf{r}$.

Exchange part ϵ_x can be calculated from Hartree–Fock exchange as

$$E_x[n] = -\frac{1}{2}\sum_{i,j}\iint d\mathbf{r}d\mathbf{r}'\frac{\phi_i^*(\mathbf{r})\phi_j^*(\mathbf{r}')\phi_j(\mathbf{r})\phi_i(\mathbf{r}')}{\mid \mathbf{r}-\mathbf{r}' \mid}$$

giving the result

$$\epsilon_x(n) = -\frac{3}{4\pi}(3\pi^2 n)^{1/3}. \tag{3.15}$$

This is first calculated by Dirac [17] as a correction to Thomas–Fermi method[3] and later by Slater [20] using HF. Unlike the exchange part, correlation energy can be calculated analytically only for certain limits of high and low density. The middle part is known from highly accurate Monte Carlo simulation calculated by Ceperley and Alder [21] and its parametrization. The most widely used one is VWN [22] and the most recent and accurate one is PW [23].

A slightly more complex version of LDA is the Local Spin Density Approximation (LSDA), which includes the local spin densties. This time the exchange–correlation energy per particle is per each spin and the functional is

$$E_{xc}^{\mathrm{LSDA}}[n] = \int d\mathbf{r}n(\mathbf{r})\epsilon_{xc}(n_\downarrow(\mathbf{r}), n_\uparrow(\mathbf{r})).$$

The LSDA is slightly better for systems having spin polarization.

From its construction, LDA is a good approximation if the density is varying slowly in which case $V_{xc}(\mathbf{r})$ has a local form. This condition makes LDA a very drastic approximation. However, LDA has proven to yield results better than expected even for systems where density is not a constant. One of the first calculation done by DFT in the frame of LDA is by Lang and Kohn[24] where surface[4] energies of some metals are calculated. The results are in agreement with experiments up to 75%. This is an improvement to HF which cannot predict the correct sign for the energies of the systems considered saying that metals are not stable. This mysterious success of the LDA is because of the error cancellation behavior of the method. LDA typically under estimates E_c but overestimates E_x and the result is surprisingly good for some of the systems. Also LDA meets the conditions necessary for an exchange–correlation functional like the sum rule by construction because the homogeneous electron gas is a real physical system [25]. This is the reason why LDA is still an option for DFT calculations.

[3] This is so called Thomas–Fermi–Dirac method and if $E_x[n]$ is multiplied by a strength parameter α then the method is the so called $X\alpha$ approximation.

[4] Surface means the density is changing very rapidly especially at the surface boundary where the periodic structure of the matter is suddenly truncated.

3.4.2 The Generalized Gradient Approximation

Although the LDA works better than predicted and become the common choice in electronic structure calculations, it is indeed insufficient for the systems having inhomogeneous density. Also the treatment of the system as an homogeneous electron gas is very drastic and has lead to search for a more accurate exchange-correlection functional. The first and very intuitive attempt is to expand the exchange–correlation energy in terms of the density (Gradient Expansion Approximation)[5]. At first glance this gradient expansion seems to yield better result because the LDA is the zeroth order term in the expansion [26];

$$E_{xc}[n] = A \int d\mathbf{r}\, n^{4/3} + C \int d\mathbf{r}\, \frac{|\nabla n|^2}{n^{4/3}} + \dots$$

where $A = -3/4(3/\pi)^{1/3}$ and $C = -7/[432\pi(3\pi^2)^{1/3}]$. However inclusion of higher order terms yields worst results than the LDA itself. The reason for this is that the exchange–correlation energy has to meet some formal conditions like exchange–correlation sum rule (equations (2)-(4) in [26]). In order to meet these conditions one has to consider only the density and its first derivative, instead of a systematic gradient expansion. This approach is the Generalized Gradient Approximation (GGA) and the exchange–correlation functional has the form

$$E_{xc}^{\mathrm{GGA}}[n] = \int d\mathbf{r}\, f(n(\mathbf{r}), \nabla n(\mathbf{r})). \tag{3.16}$$

In general the GGA is better than LDA in calculating bond dissociation energies, bulk moduli, and lattice parameters. However there is no guarantee that the GGA will be better for some specific calculation. In some systems the LDA gives better results compared to the GGA which cannot be predicted. Thus, it is always worth to check both of the two methods to be sure which one is more accurate for a certain calculation.

3.4.3 PBE Parametrization of the GGA

There is no unique way in choosing the function $f(n(\mathbf{r}), \nabla n(\mathbf{r}))$ in (3.16) and there are different GGAs only differing in the choice of this function. The most widely used ones in physics are by Perdew and Wang (PW91) [23] and Perdew, Burke and Enzerhof (PBE) [3]. PW91 is an analytic fit to the numerical GGA that is calculated starting from the second-order density-gradient expansion for the exchange–correlation hole surrounding the electron in a system of

[5] This was first suggested in the original paper [19]

slowly varying density, then cutting off its spurious long-range parts to satisfy the sum rules. But PW91 incorporates some inhomogeneity effects and has some problems listed in Ref. [3] mainly about the complexity of the analytic function, improper behavior at the high density limit which are in comparison with the LSDA approximation. What is done by PBE is that by sacrificing a correct but less important feature of PW91, which is the correct second-order gradient coefficients for exchange and correlation energies in the slowly varying density limit, correct features of LSDA are retained and combined with the gradient-corrected nonlocality. In general PBE gives very similar results as PW91 (see Table I in Ref. [3]), but PBE has a simpler form and derivation which makes it be easier to apply.

3.5 The Projected Augmented Wave Method

Projected augmented-wave (PAW) method [2] combines ideas of pseudopotential (PP) and linearized augmented plane wave methods. It is an all-electron[6] approximation giving information about all electrons of the system but not only valance electrons. The wave functions are full and the potential is determined from full charge densities.

In PAW method, space around each nucleus of the crystal is considered as two separate but linked regions, namely, *interstitial* and atomic or *augmented* region (see fig. 3.1). This separation is due to the fact that electrons orbiting close to the nucleus affected much more by the centered nuclear charge rather than the neighboring or surrounding crystal. In fact this concept is the basic for most of the electronic structure calculation methods[7] and results in separation of valance electrons from the core (core is formed by rest of the electrons and positively charged nucleus, i.e. a sphere with net positive charge and radius adjusted accordingly in calculations). This separation however destroys all information about the electrons considered in the core.

As stated in the original work a linear transformation operator is defined to transform physically relevant highly oscillating all-electron wave functions to numerically convenient pseudo

[6] An all-electron wave function is not the many-electron wave function but a full one-electron Kohn-Sham wave function

[7] Note that for PP methods separation is inevitable because at regions closer to the nucleus, oscillations in the wave function of free electron gas is very large, thus number of necessary basis functions (usually plane waves) is large which makes calculation impractical if the core electrons are not treated as an effective potential

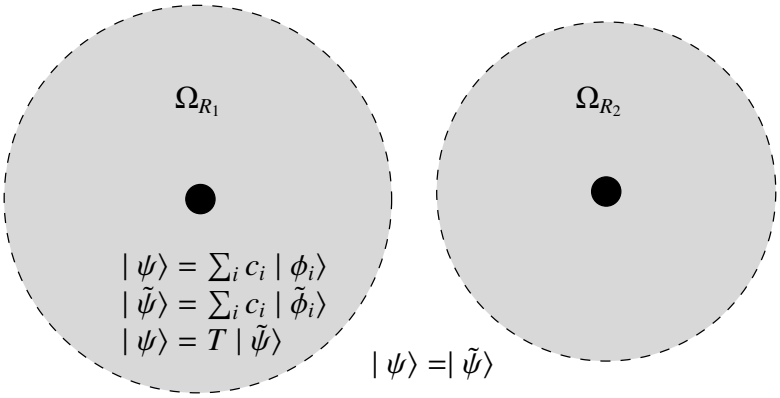

Figure 3.1: Grey circular regions are the augmentation spheres surrounding the nucleus (black points) and the remaining is the interstitial region. Transformation operator only acts in the gray circles and outside pseudo and all-electron wave functions coinside.

wave functions

$$|\psi_\lambda\rangle = T\,|\tilde{\psi}_\lambda\rangle$$

where λ denotes a certain set of quantum numbers (global index). Ground state energy can be obtained by variation with respect to these pseudo wave functions in the transformed Hilbert space

$$E_\lambda = \langle\psi_\lambda | H | \psi_\lambda\rangle = \langle\psi_\lambda | T^\dagger T H T^\dagger T | \psi_\lambda\rangle = \langle\tilde{\psi}_\lambda | \tilde{H} | \tilde{\psi}_\lambda\rangle.$$

The transformation operator is particularly chosen so that it only acts within each of the augmentation region (represented with R) where high oscillation of all-electron wave function occurs

$$T = 1 + \sum_R T_R \qquad \mathbf{r} \in \text{Augmentation region}, \qquad T(\mathbf{r}) = 0 \text{ for } r > r_c. \tag{3.17}$$

Therefore pseudo $|\tilde{\psi}\rangle$ and all-electron $|\psi\rangle$ wave functions have to coincide at interstitial region but not necessarily in augmentation region. In the augmentation region, the wave function is almost atom-like therefore it can be expanded in terms of the solutions of Schrödinger equation for the *isolated* atom. These solutions or the basis functions are called all-electron partial waves $|\phi_\lambda\rangle$.

$$|\psi_\lambda\rangle = \sum_i c_{\lambda i}\,|\phi_i\rangle.$$

In the interstitial region on the other hand, due to the periodic crystal structure there exists a periodic potential, so the solution of electronic motion is rather simpler and obtainable by PP

methods. Moreover, expansion of pseudo wave function in terms of a set of *auxiliary* functions, called pseudo partial waves $|\tilde{\phi_\lambda}\rangle$, is also possible owing to the transformation operator which can definitely transform the set of all-electron partial waves in the augmentation region.

$$|\tilde{\psi}_\lambda\rangle = \sum_i c_{\lambda i} |\tilde{\phi}_i\rangle.$$

Note that these functions per construction coinside with the corresponding all-electron partial waves $|\phi_\lambda\rangle$ at interstitial region. Applying the transformation 3.17 one can obtain T in terms of partial waves as

$$T_R |\tilde{\phi}_i\rangle = |\phi_i\rangle - |\tilde{\phi}_i\rangle \tag{3.18}$$

for a definite augmentation region R where

$$T = 1 + \sum_a T_a, \qquad T_a(r) = 0 \qquad r > r_c$$

and a is the atomic index. It is now possible to write all electron wave function as

$$\begin{aligned} |\psi_\lambda\rangle &= \sum_i c_{\lambda i} T |\tilde{\phi}_i\rangle = \sum_i c_{\lambda i}(1 + T_R) |\tilde{\phi}_i\rangle \\ &= |\tilde{\psi}_\lambda\rangle - \sum_i c_{\lambda i} |\tilde{\phi}_i\rangle + \sum_i c_{\lambda i} |\phi_i\rangle. \end{aligned} \tag{3.19}$$

Next step is to define the coefficients of the expansions which can be done by introducing projector functions $\langle\tilde{p}_i|$ such that

$$\langle\tilde{p}_i | \tilde{\phi}_i\rangle = \delta_{ij} \qquad \sum_i |\tilde{p}_i\rangle\langle\tilde{\phi}_i| = 1 \tag{3.20}$$

inside the augmentation region[8]. Therefore

$$c_{\lambda i} = \langle\tilde{p}_i | \tilde{\psi}_\lambda\rangle = \langle p_i | \psi_\lambda\rangle. \tag{3.21}$$

Substituting (3.21) into (3.19) all electron wave function with the contributions of all augmentation regions can be obtained as[9]

$$|\psi_\lambda\rangle = |\tilde{\psi}_\lambda\rangle + \sum_R \sum_i \langle\tilde{p}_i^R | \tilde{\psi}_\lambda\rangle \left(|\phi_i^R\rangle - |\tilde{\phi}_i^R\rangle \right). \tag{3.22}$$

In summary the main points of the PAW method are

[8] Note that if all electron partial waves can be constructed exactly, i.e. they are not only defined inside the augmentation regions then $|\tilde{p}_i\rangle = |\tilde{\phi}_i\rangle$.

[9] Similar procedure can be followed to calculate expectation values of observables and charge density. See the original paper [2] and a nice summary in [27] for more.

Solutions of the isolated atom is used as a basis and all-electron wave function is expanded in terms of them inside the augmentation region.

Instead of working with highly oscillating all-electron wave function, its more convenient to construct rather smoother pseudo wave function which has to coincide with the former at the interstitial region.

Projector operators (functions) is introduced in order to satisfy completeness relation inside the augmentation region.

CHAPTER 4

DESCRIPTION OF THE PROBLEM AND RESULTS

4.1 Rutile Structure

Titanium dioxide has three major crystalline structures in nature, namely rutile, anatase and brookite. Rutile and anatase are the most important crystallographic structures and rutile is the thermodynamically most stable phase. Its (110) surface has the lowest surface energy and is the most studied single-crystal TiO_2 surface [7, 28]. For this reason this particular modification of titania is chosen to be investigated.

4.1.1 The Bulk

Rutile form of titanium dioxide crystal is constructed in a tetragonal lattice together with a basis of two titanium and four oxygen atoms. There are two cell parameters, first being one side of the bottom square, a, and the second the height of the tetragon, c. Since pseudopotentials are used in the present calculations, if experimental values are used as lattice parameters then the unit cell would not be in equilibrium. Therefore cell parameters yielding the least stress on the basis atoms should be determined by looking at the change of the total energy obtained for different choices of lattice parameters. In this case there are two lattice parameters, a and c, so a coupled minimization is necessary. The following calculation is based on a series of nine volumes in the range between 1.1 and 0.83 times that of the experimental value [29] and for each volume there is a series of nine c/a ratio again between 1.1 and 0.86 times that of the experimental value. For each E versus c/a curve a cubic polynomial fit is used in order to determine the c/a corresponding to the minimum energy. Next step is to calculate total energies using this calculated minimum c/a in the corresponding volumes and fit the so–obtained

E versus V curve to the Murnaghan equation of state [30] (see Fig. 4.2). Calculated lattice parameters are listed in Table 4.1 and compared with existing data.

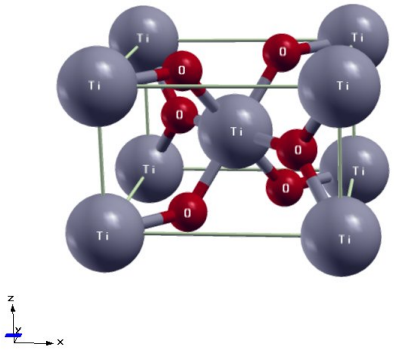

Figure 4.1: Tetragonal unit cell of TiO_2 with basis two Ti's and four O's

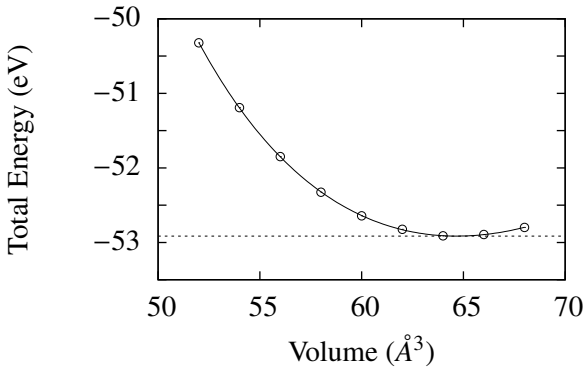

Figure 4.2: Energy versus volume using optimized values of c/a (circles) and fit to Murnaghan equation of state [30] (solid line).

From the electronic structure calculations the band structure of rutile are obtained along the high-symmetry directions of the irreducible Brillouin zone and is normalized to Fermi level. It is demonstrated with the density of states in Fig. 4.3(a). The lower valence bands are dominated by O_{2s} states where the upper valence band composed mainly of O_{2p} orbitals mixed with states of Ti_{3d}. In addition to this, the lower conduction band almost completely consists of the empty Ti_{3d} states with a very little O_{2p} mixture. The band width of the upper valence band is 5.6 eV which is in agreement with the theoretical value of 5.7 eV [32] and

Table 4.1: Structural parameters of TiO_2

Parameter	Expt.[29]	PBE-GGA [31]	This work
$a(\mathring{A})$	4.594	4.634	4.666
$c(\mathring{A})$	2.958	2.963	2.968
$u(a)$	0.305	–	0.305
$V(\mathring{A}^3)$	62.42	63.63	64.61

the experimental values which are in the range $5-6$ eV [32]. The band gap of rutile bulk is calculated to be 1.66 eV which is a direct-gap at the point Γ. The gap is largely underestimated[1] considering the experimental value of 3.03 eV [33], but it is consistent with another DFT PAW-PBE calculation done by Labat *et al.* [34] who obtained 1.69 eV as well as other ab-initio calculations that gave 1.78 eV [35], and 2.0 eV [32].

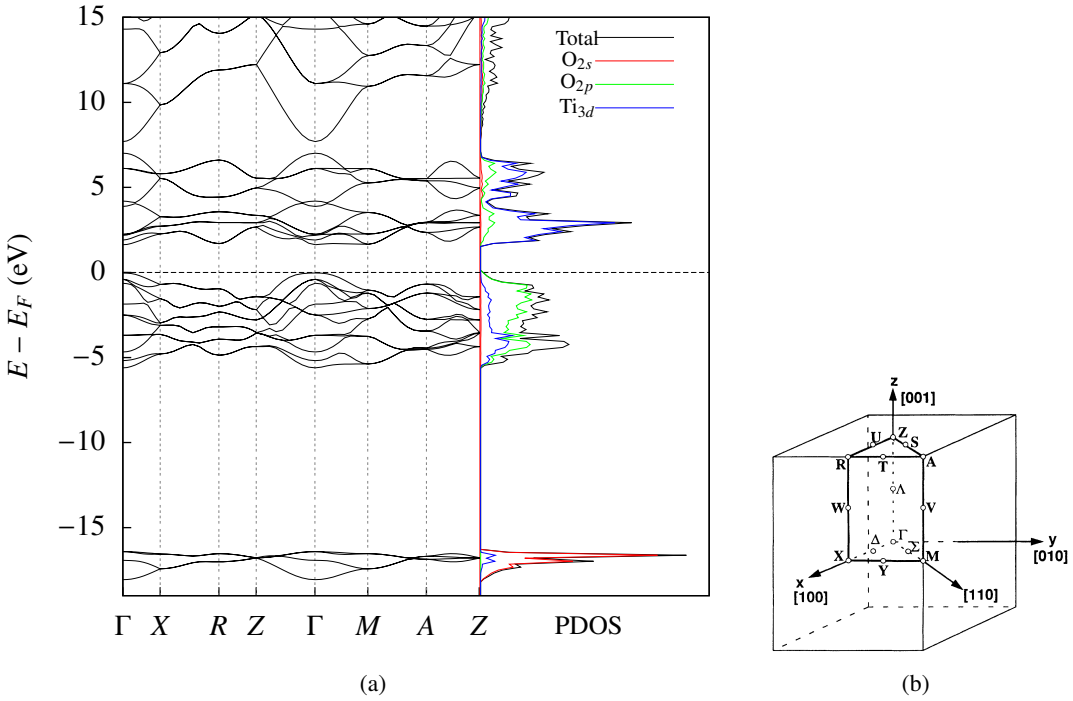

(a) (b)

Figure 4.3: Bulk energy bands for rutile along high symmetry lines in the Brillouin zone (b) (from Ref. [32]) and the corresponding partial and total DOS.

[1] In a DFT calculation the band structure is plotted from the eigenvalues of the Kohn–Sham system. But since this system is an auxiliary non-interacting system, although the density and the total energy is correct and physically meaningfull, the eigenvalues by themselves are not. Because of this the band gap is largely underestimated.

4.1.2 The (110) Surface

Unit cell of rutile (110) surface is shown in Fig. 4.4(b). It consists of two different types of oxygen and titanium atoms: Two-fold and three-fold coordinated oxygen atoms (3, and 4–7 in Fig. 4.4(b)) and five-fold and six-fold coordinated titanium atoms (2, and 1, 8, 9). The latter are connected through 3-fold oxygen atoms lying on the same plane and are called in-plane oxygen atoms. The bridging two-fold coordinated oxygen atoms sit midway between two 6-fold coordinated titanium atoms along [001] direction and form the upper most region of the surface. Bridging oxygen atoms and the 5-fold titanium atoms have dangling bonds and are the best sites for adsorption.

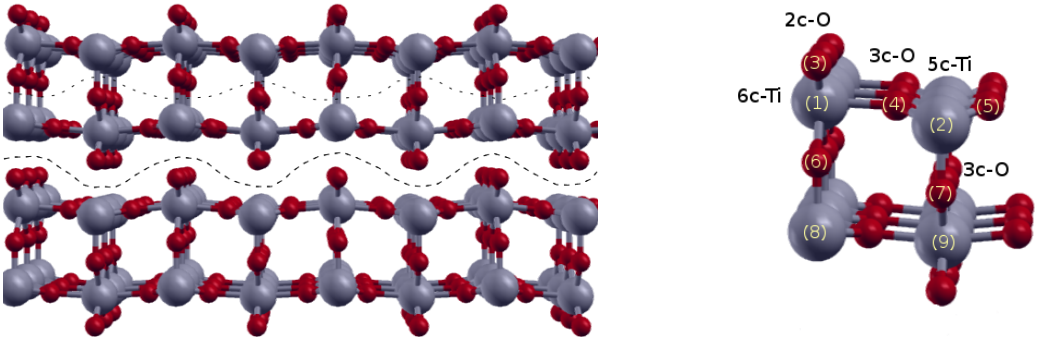

(a) (b)

Figure 4.4: In order to construct (110) surface a cut is necessary along the lower dashed line. In (a) up direction is the [110] direction where for bulk in Fig. 4.1 it is [001] and the unit between the two dash lines is one charge-neutral surface layer; in (b) one unit cell of rutile (110) surface is demonstrated. Labels are introduced for later use in Table 4.2.

Calculations are done using a surface unit cell constructed from a 3×1 orthogonal surface slab with dimensions a = 8.90 Å and b = 6.60 Å. There are 24 titanium atoms and 48 oxygen atoms in the cell and there is a periodicity along x ([001]) and y ([1$\bar{1}$0]) directions. In order to prevent top-bottom interactions about 11 Å of vaccum is introduced along z ([110]) direction, which is an adequate value compared with the recommended 4 Å [36]. In other words, the surface is modelled in a repeated slab geometry. Each slab is thick enough and separated from the neighboring by a vacuum thick enough in z direction, thereby guarantying the repeated surfaces defining the slab do not interact with each other.

Relaxation of the surface is a rather controversial topic especially when explaining the displacements of the surface atoms. Although the directions are predicted as the same, amount

of the displacements vary depending on calculation method. The most important factor is the slab thickness which has a direct impact on the surface relaxation as the displacement of the titanium atoms on the top and bottom layers affect each other. In a slab with even number of layers, 5-fold surface titanium atoms are located above the bottom 6-fold titanium atoms. This causes them to relax more and to move deeper along [110] direction. On the contrary when the number of layers is odd 5-fold titanium atoms of top and bottom layers are paired resulting in an opposition and smaller amount of relaxation. This also holds for the 6-fold titanium atoms and since the bridging oxygen atoms are bonded to 6-fold titanium atoms, they exhibit similar behavior. As the number of layers increases this coupling between the top and bottom surface loses its strength especially after the critical value of four [36]. Therefore it is important to have similar setups in the number of layers when a comparison has to be made. Because of this although in this study a four-layer slab is used, to make a comparison a seven-layer surface is constructed with the same cell parameters and the results of the relaxation are listed in Table 4.2. For the comparison Ref. [36] is chosen because it is done with VASP code and GGA exchange-correlation potential[2]. Also an x-ray diffraction experiment is included for comparison. Since there is almost no displacement along x and y directions ([001] and [1$\bar{1}$0]), the listed values are along [110] direction except for the in-plane oxygen atoms (4 and 5). Calculations show that 6-fold titanium atoms go up and 5-fold go down with in-plane oxygen atoms compensating this through an upward motion. Bridging oxygen atoms seem to be not relaxing at all. Comparison with the theoretical study seems reasonable but agreement with the experimental results is half assured worst being the bridging oxygen displacement. The reason for this is that in the calculations the positions of the nuclei can be calculated exactly whereas for the x-ray diffraction experiments electron density distribution is measured and positions of the nuclei are guessed through this information. However unlike titanium atoms where the electrons are tightly bound to core states, highly asymmetric bridging oxygen atoms may create a polarization on the valence electrons because most of them are in 2s and 2p valence states. The nucleus and the valence electrons are localized at different spatial positions leading to the discrepancy.

Fig. 4.5 presents both the band structure and DOS of rutile (110) surface calculated using the 4-layer unit cell. Also local DOS for the surface atoms are included and multiplied by

[2] For more comparisons see [7] p. 72–74.

Table 4.2: Displacement ($\mathring{A}$) of ions at the surface layer with comparisons

	This work (PBE-GGA)	PW91-GGA[36]	Experiment [37]
Ti(1)	0.21	0.23	0.12 ± 0.05
Ti(2)	−0.18	−0.11	−0.16 ± 0.05
Ti(8)	0.15	0.12	0.07 ± 0.04
Ti(9)	−0.10	−0.06	−0.09 ± 0.04
O(3)	0.02	−0.02	−0.27 ± 0.08
O(4), O(5)			
(along [110])	0.16	0.18	0.16 ± 0.08
(along [1$\bar{1}$0])	±0.05	±0.05	±0.05 ± 0.05
O(6)	0.01	0.03	0.03 ± 0.08
O(7)	0.00	0.03	0.00 ± 0.08

a factor of two to see the contributions more clearly. The case is similar to the bulk, that is upper valence band contributions are mainly due to O-2p states and lower conduction bands are due to Ti-3d states. Surface atoms contribute to the band structure largely at the edges of valence and conduction bands.

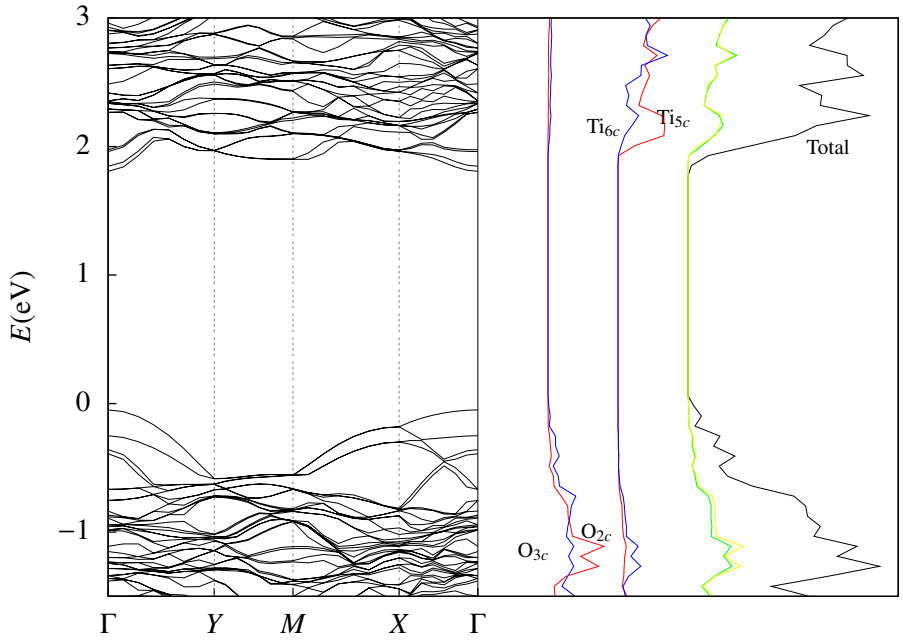

Figure 4.5: Band structure of rutile (110) 3 × 1 surface with total DOS and local DOS of surface atoms (red and blue curves) and top–bottom surface (green and yellow curves). All LDOS values are multiplied by a factor of 2 for convenience. Here O_{2c} is 3, O_{3c} is 4-5, Ti_{5c} is 2 and Ti_{6c} is 1 in Fig. 4.4(b).

4.2 Anchor Groups

Some organic molecules and dyes can be directly adsorbed on the surface but the molecules studied in this work are very stable[3] and unlikely make chemical bonds with the surface. It is thus more convenient to choose smaller functional groups for bonding. Since these groups link the large molecule and the surface they are called anchor groups. Most importantly these molecules assure a strong adsorption and easy to guess adsorption geometry because the conncetion can only be done through the oxygen atoms and hydroxyl group of acids for which the best adsorption site on the surface is over five-fold coordinated titanium atoms (metal–oxygen bond) and the bridging oxygen atoms (hydrogen bond). Since the interaction between master molecule, anchor and the surface has a fundamental role, knowledge of the geometry and the strength of the bonds are crucial in application.

Carboxylic groups are frequently used as the anchors since photosensitizers are often synthesized with carboxylic acid groups. One of the anchor groups used in this study is formic acid that is the simplest carboxylic acid. Following the experimental findings [39] (and ref within) there are mainly two favorable adsorption sites. The first one provides binding between 5-fold titanium and the formic oxygen; 2-fold surface oxygen and the hydroxyl hydrogen of the formic acid. This configuration is called monodentate binding (see Fig. 4.6(a)). The second one includes two bonds that are between 5-fold titanium atoms and two oxygen atoms of formic acid, but in this case formic acid is disassociated on the surface giving its hydroxyl hydrogen to 2-fold surface oxygen. This is the bidantate binding (see Fig. 4.6(b)) and much more favorable than the former whose adsorption energy is lower (see Table 4.3). This is the reason why the aromatic rings are studied with the bidantate setup of formic acid (and also phosphonic acid).

Carboxylic acids are highly efficient in solar cell applications but they slowly desorb from the surface in the vicinity of water [40]. An alternative to carboxylic acids may be phosphonic acids which are less well-known than carboxylics not famous and have less studies reported. In fact phosphonic acid groups are promissing candidates as an anchor group which can also be used to bind a wide range of molecules to rutile surface. Following an intuitive approach and the experimental studies refered in [40] monodantate and bidantate configura-

[3] An example may be the Ref. [38] which investigates adsorption of benzene on rutile [110] and the calculations show that adsorption energy is low (0.6 eV).

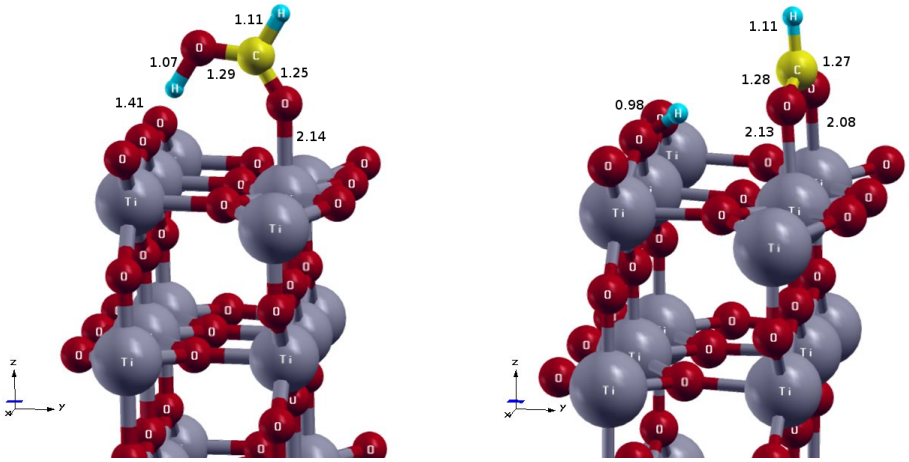

(a) Monodentate Binding (b) Bidentate Binding

Figure 4.6: HCOOH adsorbed on rutile TiO_2(110)–3×1 surface.

tions of formic acid can be applied to phosphonic acid adsorption (see Fig. 4.7(a) 4.7(b)). The bidantate binding is more favorable with greater adsorption energy as predicted (Table 4.3). Again there is a dissociation for this geometry where one of the hydroxyl hydrogen captured by 2-fold surface oxygen creating another metal-oxygen bond with 5-fold titanium. The crucial point is that the difference between the adsorption energies of the two groups is large and phosphonic acid links the master molecule strongly to the surface which is the major role of an anchor.

Electronic structure calculations show that all molecular orbital levels are merged into the rutile valence band for both anchor groups. This indicates that there exists a strong electronic coupling with the surface meaning that the anchors are good adsorbates. The adsorption of the anchor groups does not shift or change the size of the band gap significantly, compared to the corresponding clean surface (see Fig. 4.14 and 4.13).

4.3 Aromatic Rings Bound to TiO_2 Surface through the Anchors

Aromatic hydrocarbons have a very important role in organic chemistry. They are classified according to the number of benzene rings that they contain. The name of this class of molecules come from the fact that many of them have strong aromas which is due to a delocalized orbital created by the circular arrangement of carbon atoms bonded through alternating

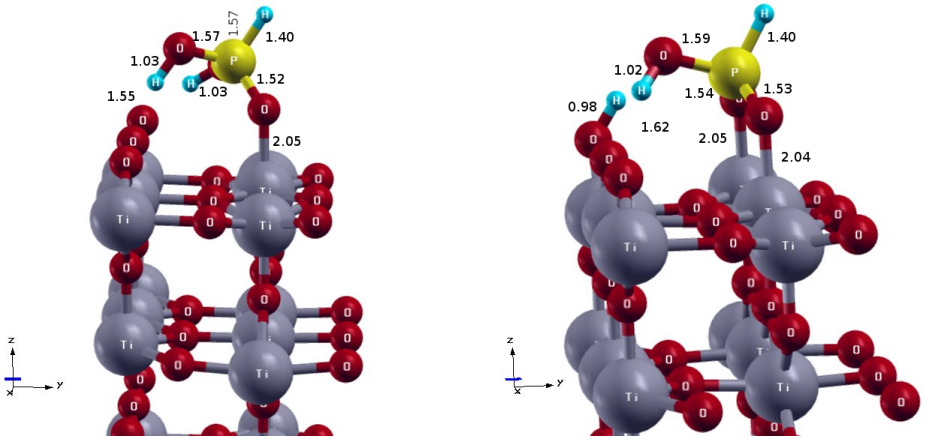

(a) Monodentate Binding (b) Bidentate Binding

Figure 4.7: HPO_3H_2 adsorbed on rutile TiO_2(110)–3×1 surface

Table 4.3: Adsorption energies (eV) of the anchor groups for different binding geometries

Anchor Group	Monodentate binding	Bidentate binding
Formic acid		
This work (PBE-GGA)	1.134	1.299
Ref. [39] (PW91-GGA)	1.243	1.358
Phosphonic acid		
This work (PBE-GGA)	1.786	2.025
Ref. [41] (HF-DFT hybrid)	2.428	2.602

double and single bonds. Rather than a localized single–double bond pattern a delocalized circular shaped orbital as combinations of the π-bonds normal to the plane of the ring exists which is proven by the fact that all six carbon–carbon bonds have the same length lying between that of a single and that of a double carbon–carbon bonds (see Fig. 4.8).

In this study a group of dye molecules that are linearly formed by a number of benzene rings are investigated. There are five different aromatic hydrocarbons that have been studied on the rutile (110) 3×1 surface. As stated earlier these are attached to the surface not directly but via formic or phosphonic acid groups which act as anchors. The orientation of the dye relative to the TiO_2 surface was determined by the direction of the nonbonded hydrogen (top hydrogen) of the acids. An overview of these molecules is shown in the Fig. 4.9. Tetracene and pentacene are the most important ones among them since they can be used as models

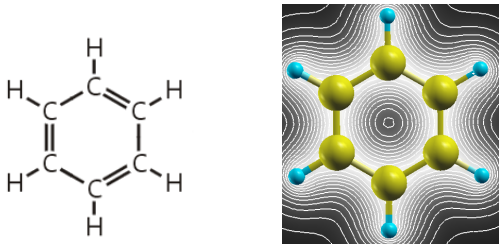

Figure 4.8: Schematic diagram of benzene ring and charge density plot. Circular charge density inside the ring indicates one delocalized circular bond instead of alternating single and double carbon–carbon bonds.

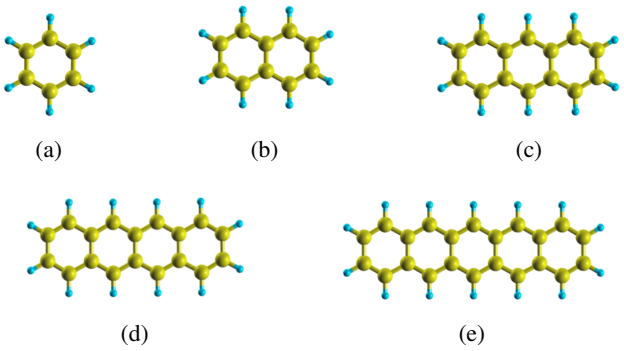

Figure 4.9: Dye molecules with linearly connected aromatic rings: (a) benzene (C_6H_6), (b) naphthalene ($C_{10}H_8$), (c) anthracene ($C_{14}H_{10}$), (d) tetracene ($C_{18}H_{12}$), and (e) pentacene ($C_{22}H_{14}$)

for the investigations of electron transfer in dye–metal oxide interfaces (a similar molecule perylene is investigated in Ref. [41] for such purposes).

The adsorbate–substrate bond lengths are very similar to the adsorbate–substrate bond lengths for adsorption of only the anchor group. The notable difference in the optimized geometries occurs for the adsorption through phosphonic acid. Each molecule has a tilt from the surface normal orienting the long axis of the molecule at angle of about 20°. On the other hand all molecules adsorbed through formic anchor preserved both the bond lengths and the angle (tilt is smaller than 2°) due to the upright orientation of the formic acid. A similar result has been observed for some perylene based dyes bound to rutile (110) surface through the two anchor groups [42].

Adsorption energies of aromatic rings which is bound to the surface via anchors are listed in Table 4.4. The calculated adsorption energies are comparable to the energies for adsorption of anchor group alone (Table 4.3). As an expected result the rings are bond more strongly

Table 4.4: Adsorption Energies (eV) of the [Dye molecules]-[Anchor group] on (TiO_2)

Number of Rings	Formic acid	Phosphonic acid
1	1.271	1.697
2	1.254	1.761
3	1.262	1.685
4	1.258	1.682
5	1.292	1.692

through the phosphonic acid than through formic acid.

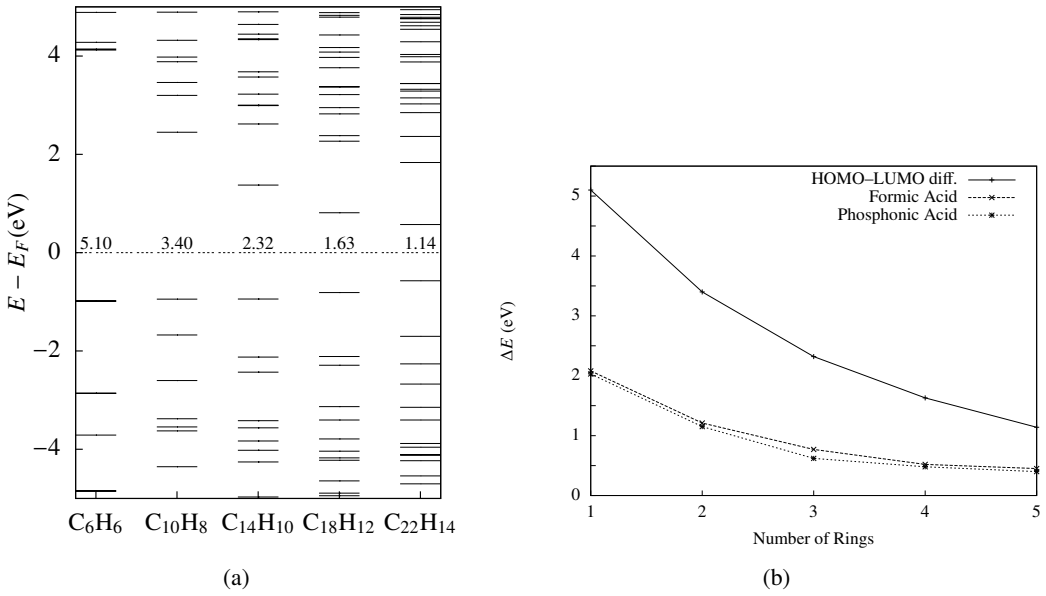

Figure 4.10: In (a) molecular levels (KS orbitals) of the dye molecules are represented. The numbers denote the energy difference between HOMO and LUMO levels of each molecule. The plot in (b) is ΔE, the energy difference between the HOMO of dyes and the conduction band edge of rutile, versus the number of rings and the HOMO–LUMO difference of dyes versus the number of rings they have.

Total and Local–DOS are presented in Fig. 4.13 for clean, anchor adsorbed and ring adsorbed configurations. Clean surface contains large amount of valence and conduction states separated by a large band gap (considering the underestimation of DFT). Although anchor groups by themselves does not introduce any states in the band gap, with a ring number greater than two there are occupied molecular levels in the gap. This is because the Fermi level is always seen to be located just above of these molecular levels, thus they are the HOMO of the system. From the band plots (Fig. 4.14) and the charge density plots (Fig. 4.15 and 4.17) it can be

concluded that there exists no coupling between the surface and the aromatic molecules with more than one ring. The coupling is only done by the used anchor group. For the case of benzene, the HOMO of the molecule lies inside the valence band and it is hardly distinguishable from the valence states, thus the states of benzene ring is in resonance with the surface valence. Also charge densities show that the HOMO levels are π-orbitals of the aromatic rings and are delocalized being extended over the whole formic acid while this is partly seen for the phosphonic group.

Table 4.5: Calculated energy values (all in eV) for the HOMO level E_{HOMO}, the LUMO level E_{LUMO}, and HOMO–LUMO energy difference $\Delta E_{H\text{-}L}$ of the molecules in gas phase.

	E_{HOMO}	E_{LUMO}	ΔE_{H-L}
C_6H_6	−5.77	−0.67	5.10
$C_{10}H_8$	−4.57	−1.17	3.40
$C_{14}H_{10}$	−3.87	−1.55	2.32
$C_{18}H_{12}$	−3.39	−1.76	1.63
$C_{22}H_{14}$	−3.74	−2.60	1.14
C_6H_6-COOH	−5.99	−2.01	3.98
$C_{10}H_8$-COOH	−5.22	−2.10	3.12
$C_{14}H_{10}$-COOH	−4.59	−2.37	2.22
$C_{18}H_{12}$-COOH	−4.13	−2.56	1.57
$C_{22}H_{14}$-COOH	−3.80	−2.68	1.12
C_6H_6-PO_3H_2	−6.05	−1.51	4.54
$C_{10}H_8$-PO_3H_2	−5.13	−1.83	3.30
$C_{14}H_{10}$-PO_3H_2	−4.47	−1.18	2.29
$C_{18}H_{12}$-PO_3H_2	−4.01	−2.41	1.60
$C_{22}H_{14}$-PO_3H_2	−3.68	−2.55	1.13

The HOMO–LUMO difference of the adsorbates are the same as the gas phase of anchored aromatic rings irrespective of anchor group. There is a slight difference between the HOMO–LUMO gap of rings alone and the (adsorbed) anchored rings for number of rings greater than four and this difference is noticible for smaller number of rings being largest for benzene. The HOMO–LUMO′[4] difference is almost the same with the gas phase of the anchored and isolated rings although the HOMO and LUMO levels are different. This may be due to the conclusion that the rings are not interacting with the surface but the anchor groups are. The delocalization of the LUMO over the anchors results in LUMO′ level alignment. As the delocalization extended, the LUMO′ level lowering, in other words, bindings through formic acid have lower LUMO′ level which is due to the extended LUMO over the group. This can

[4] LUMO′ is the LUMO level of the adsorbed molecule obtained from LDOS plots of the combined systems.

Table 4.6: Calculated energy values (all in eV) for valence band maximum V_{max}, conduction band minimum C_{min}, band gap E_g, and HOMO–LUMO′ energy difference $\Delta E_{H\text{-}L'}$ of the adsorbates.

	V_{max} or E_{HOMO}	C_{min}	E_g	$E_{LUMO'}$	$\Delta E_{H\text{-}L'}$
TiO_2(110)–3 × 1 slab	−2.51	−0.65	1.86	-	-
C_6H_6-COOH-(TiO_2)	−2.67	−0.84	1.83	1.36	4.25
$C_{10}H_8$-COOH-(TiO_2)	−2.12	−0.89	1.23	1.04	3.10
$C_{14}H_{10}$-COOH-(TiO_2)	−1.79	−1.03	0.76	0.35	2.11
$C_{18}H_{12}$-COOH-(TiO_2)	−1.54	−1.01	0.53	−0.02	1.53
$C_{22}H_{14}$-COOH-(TiO_2)	−1.43	−0.97	0.46	−0.26	1.07
C_6H_6-PO_3H_2-(TiO_2)	−2.70	−0.90	1.80	1.91	4.79
$C_{10}H_8$-PO_3H_2-(TiO_2)	−2.10	−0.95	1.15	1.21	3.25
$C_{14}H_{10}$-PO_3H_2-(TiO_2)	−1.61	−0.99	0.62	0.69	2.26
$C_{18}H_{12}$-PO_3H_2-(TiO_2)	−1.41	−0.95	0.46	0.22	1.57
$C_{22}H_{14}$-PO_3H_2-(TiO_2)	−1.31	−0.90	0.41	−0.13	1.14

also be seen from the PDOS plots Fig. 4.13 in addition to the values listed in the Table 4.6.

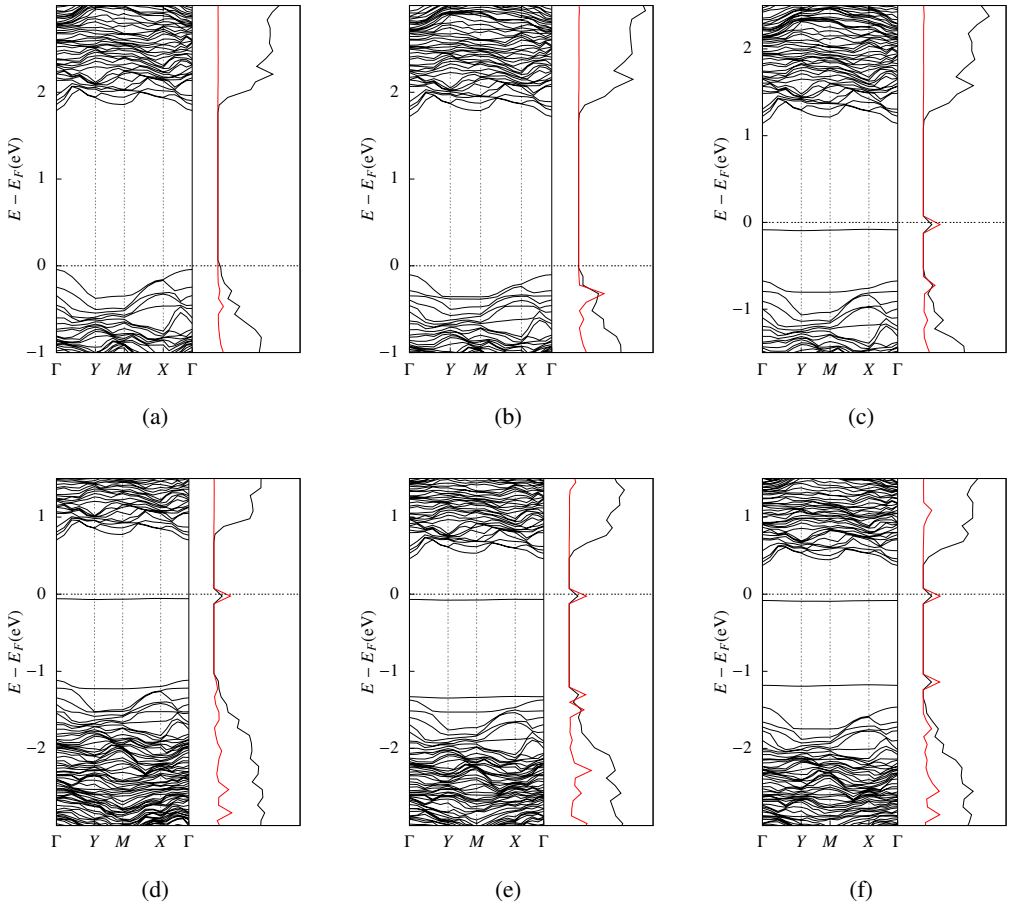

Figure 4.11: Band structures with total and local DOS for (a) COOH-(TiO_2), (b) [benzene]-COOH-(TiO_2), (c) [naphthalene]-COOH-(TiO_2), (d) [anthracene]-COOH-(TiO_2), (e) [tetracene]-COOH-(TiO_2), and (f) [pentacene]-COOH-(TiO_2). All local DOS curves (in red) are multiplied by 2

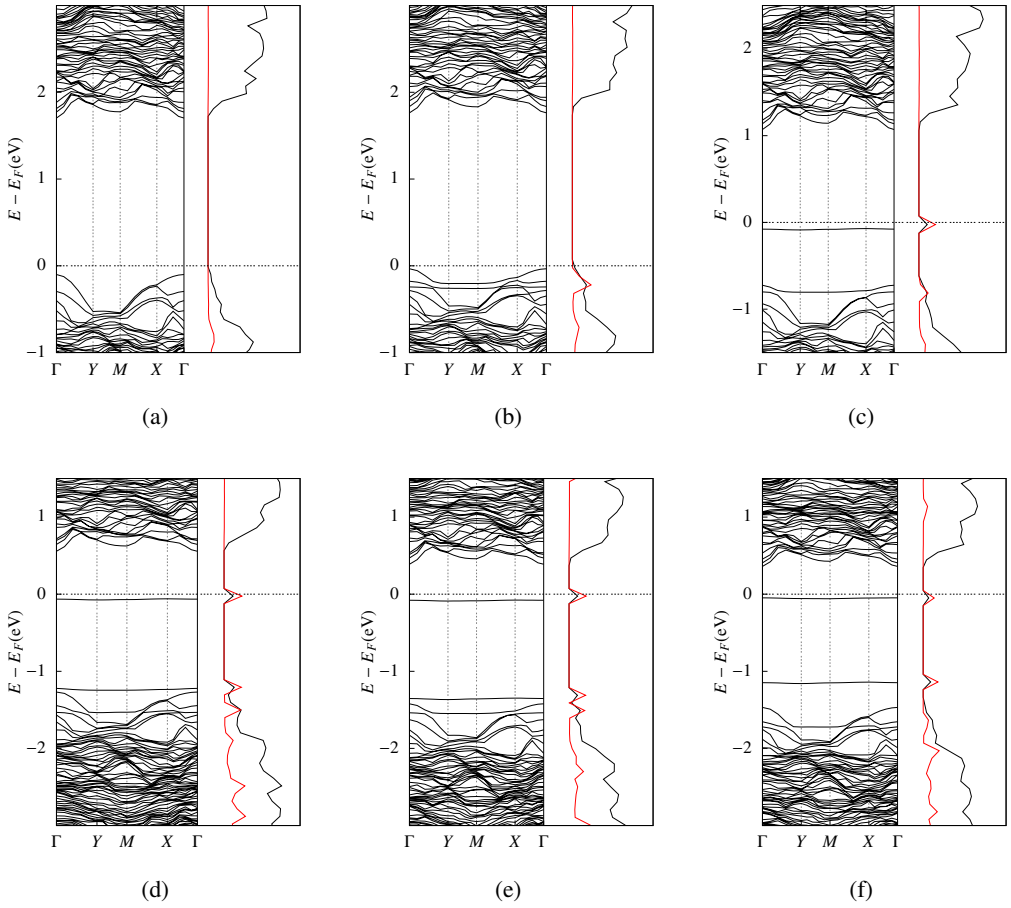

Figure 4.12: Band structures with total and local DOS for (a) PO_3H_2-(TiO_2), (b) [benzene]-PO_3H_2-(TiO_2), (c) [naphthalene]-PO_3H_2-(TiO_2), (d) [anthracene]-PO_3H_2-(TiO_2), (e) [tetracene]-PO_3H_2-(TiO_2), and (f) [pentacene]-PO_3H_2-(TiO_2). All local DOS curves (in red) are multiplied by 2.

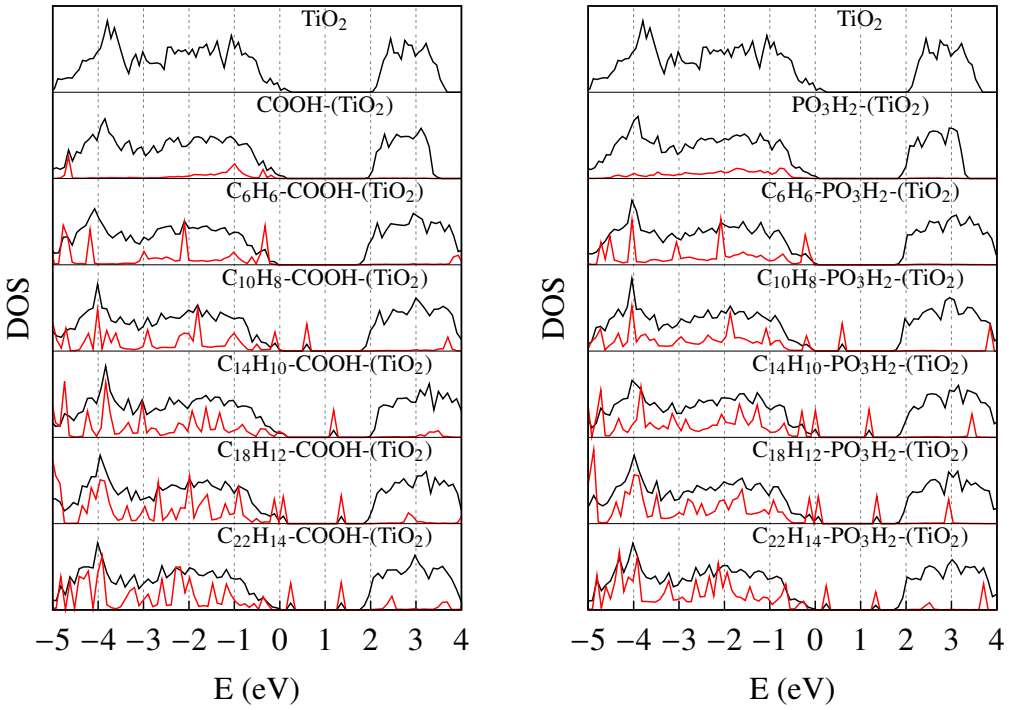

Figure 4.13: Total DOS (black) and adsorbate-projected DOS (red) for (a) aromatic rings bound through formic acid and (b) through phosphonic acid. All LDOS curves (in red) are multiplied by 4.

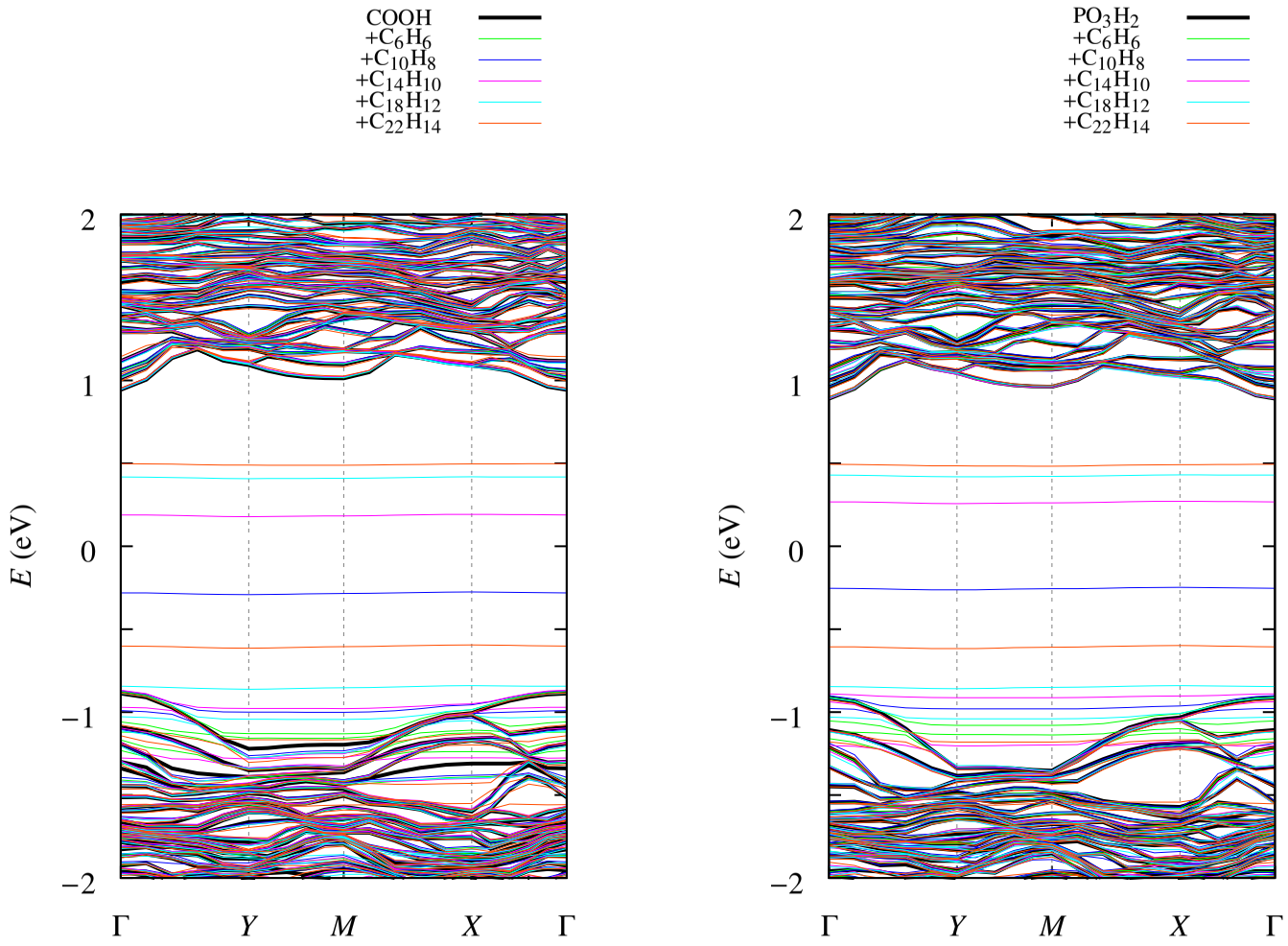

Figure 4.14: Band structures for all cases are plotted in a single graph for each system (a) [Dye]-COOH-(TiO_2) and (b) [Dye]-PO_3H_2-(TiO_2). Conduction and valence band contributions do not differ much, main difference is in the flat-like bands (usually corresponding to HOMO and below levels) that fall into the bulk bandgap.

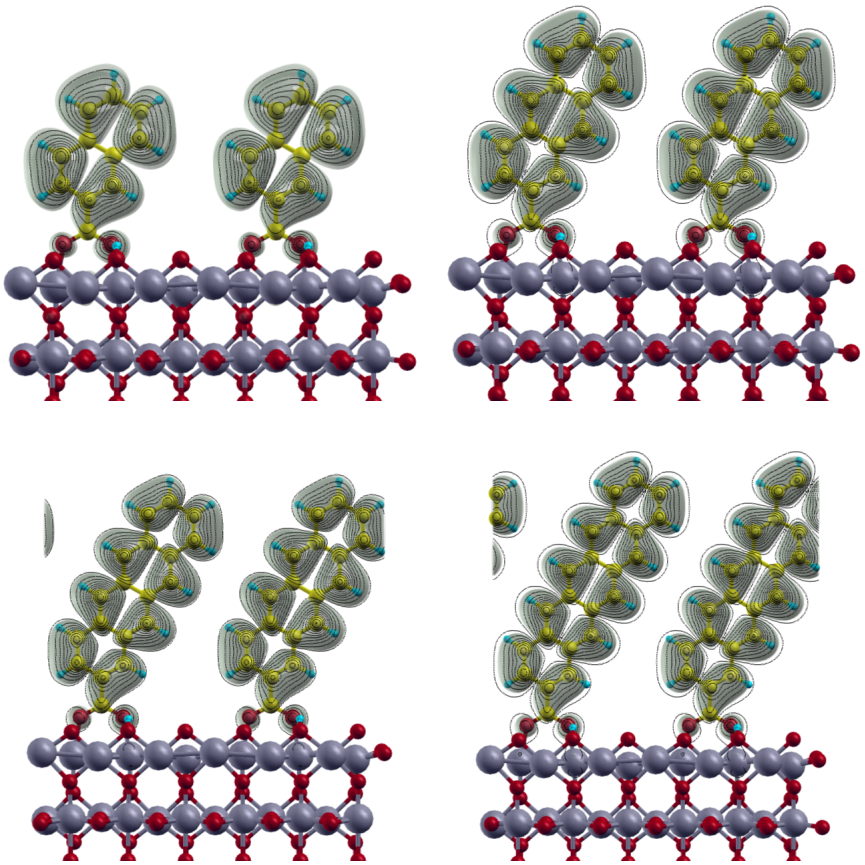

Figure 4.15: Calculated Γ-point partial charge densities of HOMO of Dye-COOH-(TiO_2)

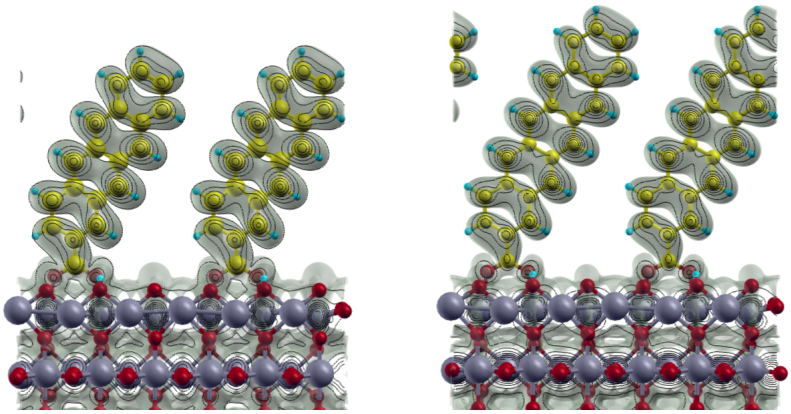

Figure 4.16: Calculated Γ-point partial charge densities of LUMO′ of [Tetracene and Pentacene]-COOH-(TiO_2). Notice the contours between the anchor group and the first ring indicating delocalization of the LUMO level.

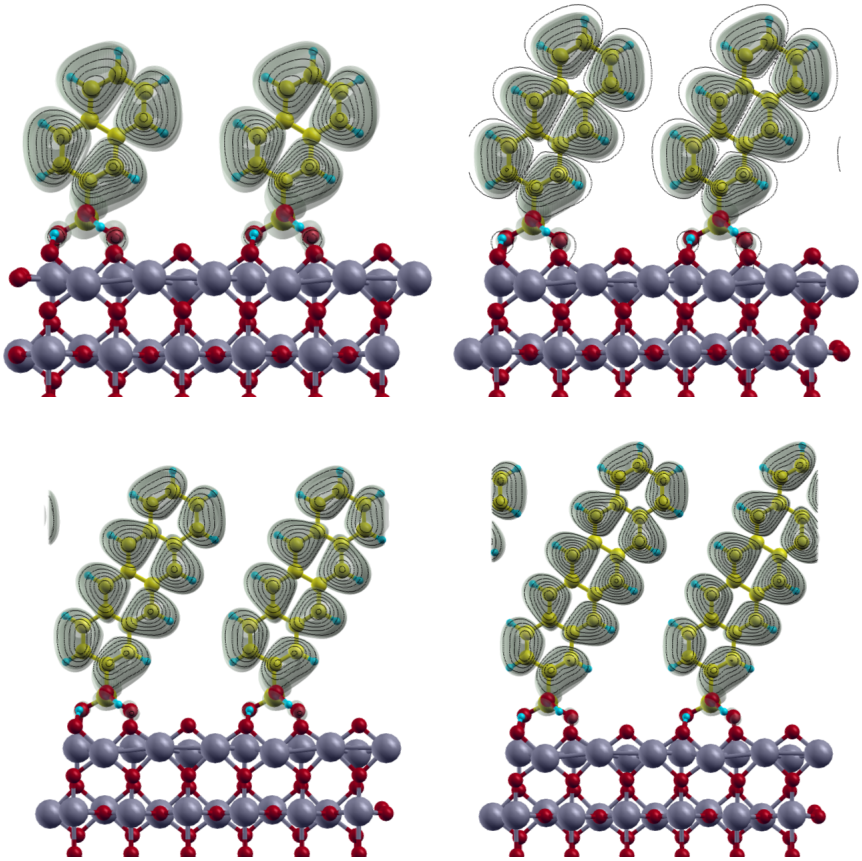

Figure 4.17: Calculated Γ-point partial charge densities of HOMO of Dye-PO_3H_2-(TiO_2)

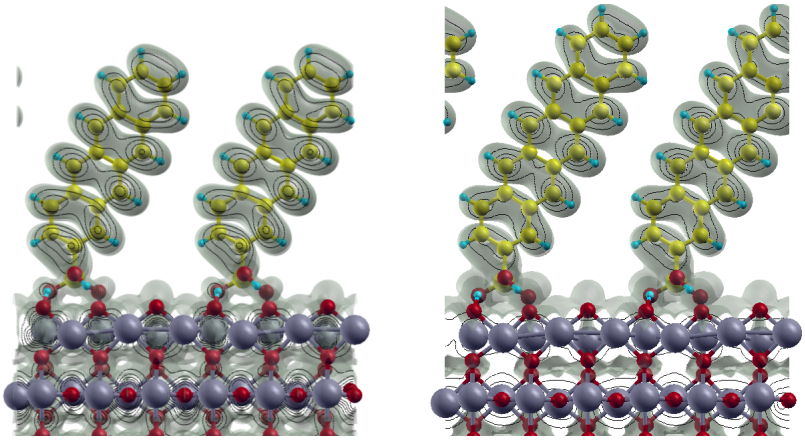

Figure 4.18: Calculated Γ-point partial charge densities of LUMO′ of [Tetracene and Pentacene]-PO_3H_2-(TiO_2).

4.4 Conclusion

In order to study a dye-sensitized solar cell system, one has to know interfacial electronic coupling of the dye or the spacer groups used for binding (see Appendix 1.1). In this work this is done for aromatic hydrocarbons up to five benzene rings (pentacene), which are the main constituents of the organic dyes. These are linked to the surface with two different anchors in order to strengthen adsorption and electronic coupling. After comparing the unit cell parameters and relaxation of the constructed surface model with the experiment and other calculations, electronic structure calculations of dyes bound to the rutile surface through formic and phosphonic anchor groups have been conducted and some remarks are as follows;

- Both of the anchor groups have greater adsorption energies (adsorbs strongly to the surface) for the bidantate setups. This is mainly due to the dissociation of the hydroxyl hydrogen of the anchor groups over the surface (which then binds to a bridging oxygen) and two metal–oxygen bindings.
- Formic acid binds more loosely than phosphonic acid which can be seen from the adsorption energies and the difference is about 0.7 eV. On the otherhand, the adsorption of formic acid can still be considered as strong with the adsorption energy as big as 1.3 eV.
- Adsorption properties of the aromatic rings are found to be determined by the adsorption properties of the anchor group itself. This is understandable from the adsorption energies listed in Table 4.4 and Table 4.3. Because of the greater adsorption energy of phosphonic acid, all of the rings are bond to the surface stronger than with formic acid.
- The HOMO and the LUMO′ levels of the combined systems are delocalized over formic acid anchor which indicates stronger interfacial electronic coupling. This is the greatest advantage of using formic acid as the anchor in addition to its fame that many of the efficient ruthenium based dyes constitutes formic acid anchoring [6], [9]. Also the LUMO′ levels are lower when formic acid is used especially for number of rings up to four. Lower LUMO levels lead to lower gap between π and π^* levels of the aromatic rings.
- Anchor group addition to the rings lessens the HOMO–LUMO difference and this lowering is larger for formic acid with ring number smaller than four. The gap of the com-

bined system is decreasing with the increasing ring number although the HOMO levels are not changing largely (see Fig. 4.10(a)). The decrease in the gap is greatly affected from the HOMO–LUMO difference of the rings alone (see Fig. 4.10(b)). Also the HOMO–LUMO′ difference of the combined system is very similar to HOMO–LUMO difference of anchored rings (see Table 4.6).

REFERENCES

[1] Hohenberg, P. & Kohn, W. Inhomogeneous Electron Gas. *Phys. Rev.* **136**, B864 (1964).

[2] Blöchl, P. E. Projector Augmented-Wave Method. *Phys. Rev. B* **50**, 17 953 (1994).

[3] Perdew, J. P., Burke, K. & Ernzerhof, M. Generalized Gradient Approximation Made Sipmle. *Phys. Rev. Lett.* **77**, 3865 (1996).

[4] Kresse, G. & Furthmuller, J. Efficient iterative schemes for ab initio total-energy calculations using a plane-wave basis set. *Phys. Rev. B* **54**, 11169 (1996).

[5] Kokalj, A. Computer graphics and graphical user interfaces as tools in simulations of matter at the atomic scale. *Comp. Mat. Sci.* **28**, 155 (2003).

[6] O'Regan, B. & Grätzel, M. A Low-Cost, High-Efficiency Solar Cell Based on Dye-Sensitized Colloidal TiO_2 Films. *Nature* **353**, 737 (1991).

[7] Diebold, U. The Surface Science Of Titanium Dioxide. *Surf. Sci. Rep.* **48**, 53 (2003).

[8] Linsebigler, A. L., Lu, G. & Jr., J. T. Y. *Chem. Rev.* **95**, 735 (1995).

[9] Hagfeldt, A. & Grätzel, M. Light-induced redox reactions in nanocrystalline systems. *Chem. Rev.* **95**, 49 (1995).

[10] Born, M. & Oppenheimer, J. R. Zur Quantentheorie der Molekeln. *Ann. d. Physik* **84**, 457 (1927).

[11] Griffiths, D. J. *Introduction to Quantum Mechanics*, 293–314 (Pearson Prentice Hall, Inc., 2005), 2 edn.

[12] Springborg, M. *Methods of Electronic-Structure Calculations*, 21–35 (John Wiley & Sons, Ltd, 1994).

[13] Feynman, R. P. Forces in Molecules. *Phys. Rev.* **56**, 340 (1939).

[14] Thomas, L. H. The Calculation of Atomic Fields. *Proceedings of the Cambridge philosophical society* **23**, 542 (1927).

[15] Fermi, E. Statistical Method of Investigating Electrons in Atoms. *Zeitschrift für Physik* **48**, 73 (1928).

[16] Lundqvist, S. & March, N. H. *Theory of The Inhomogeneous Electron Gas*, 1–75 (Plenum Press, New York, 1983).

[17] Dirac, P. A. M. Note on Exchange Phenomena in The Thomas Atom. *Proc. Cambridge Phil. Soc.* **26**, 376 (1930).

[18] Lewis, H. W. Fermi-Thomas Model With Correlations. *Phys. Rev.* **111**, 1554 (1958).

[19] Kohn, W. & Sham, L. J. Self-Consistent Equations Including Exchange and Correlation Effects. *Phys. Rev.* **146**, A1133 (1965).

[20] Slater, J. C. A Simplification of The Hartree–Fock Method. *Phys. Rev.* **81**, 385 (1951).

[21] Ceperley, D. M. & Alder, B. J. Ground State of The Electron Gas by A Stochastic Method. *Phys. Rev. Lett.* **45**, 566 (1980).

[22] Vosko, S. H., Wilk, L., & Nusair, M. Accurate spin-dependent electron liquid correlation energies for local spin density calculations: a critical analysis. *Can. J. Phys.* **58**, 1200 (1980).

[23] Perdew, J. P. & Wang, Y. Accurate and Simple Representation of The Electron-Gas Correlation Energy. *Phys. Rev. B* **45**, 13244 (1992).

[24] Lang, N. D. & Kohn, W. Theory of Metal Surfaces: Charge Density and Surface Energy. *Phys. Rev. B* **1**, 4555 (1970).

[25] Capelle, K. A bird's-eye view of density-functional theory. *arXiv:cond-mat/0211443* (2006).

[26] Perdew, J. P. & Wang, Y. Accurate and simple density functional for the electronic exchange energy: Generalized gradient approximation. *Phys. Rev. B* **33**, 8800 (1986).

[27] Holzwarth, N. A. W., Matthews, G. E., Dunning, R. B., Tackett, A. R. & Zeng, Y. Comparison of the projector augmented-wave, pseudopotential, and linearized augmented-plane-wave formalisms for density-functional calculations of solids. *Phys. Rev. B* **55**, 2005 (1997).

[28] Pang, C. L., Lindsayb, R. & Thornton, G. Chemical Reactions on rutile TiO_2(110). *Chem. Soc. Rev.* **37**, 2328 (2008).

[29] Grant, F. A. Properties of rutile (titanium dioxide). *Rev. Mod. Phys.* **31**, 646 (1959).

[30] Murnaghan, F. D. The Compressibility of Media Under Extreme Pressures. *Proc. Natl. Acad. Sci. USA* **30**, 244 (1944).

[31] Lazzeri, M., Vittadini, A. & Selloni, A. Structure and energetics of stoichiometric $TiO2$ anatase surfaces. *Phys. Rev. B* **63**, 155409 (2001).

[32] Glassford, M. K. & Chelikowsky, J. R. Structural and electronic properties of titanium dioxide. *Phys. Rev. B* **46**, 1284 (1992).

[33] Pascual, J., Camassel, J. & Mathieu, H. Fine structure in the intrinsic absorption edge of ti$o2$. *Phys. Rev. B* **18**, 5606 (1978).

[34] Labat, F., Baraneka, P., Domain, C., Minot, C. & Adamo, C. *J. Chem. Phys.* **126**, 154703 (2007).

[35] Mo, S. & Ching, W. Y. Electronic and optical properties of three phases of titanium dioxide: Rutile, anatase, and brookite. *Phys. Rev. B* **51**, 13023 (1995).

[36] Bates, S. P., Kresse, G. & Gillan, M. J. A systematic study of the surface energetics and structure of TiO_2(110) by first-principles calculations. *Surf. Sci.* **385**, 386 (1997).

[37] Charlton, G. *et al.* Relaxation of TiO_2(110)-(1×1) Using Surface X-Ray Diffraction. *Phys. Rev. Lett.* **78**, 495 (1997).

[38] Zhou, J. *et al.* Adsorption, desorption, and dissociation of benzene on tio_2(110) and pd/tio_2(110): Experimental characterization and first-principles calculations. *Phys. Rev. B* **74**, 125318 (2006).

[39] Ojamäe, L., Aulin, C., Pedersen, H. & Käll, P. IR and quantum-chemical studies of carboxylic acid and glycine adsorption on rutile TiO_2 nanoparticles. *J. Colloid Interf. Sci.* **296**, 71 (2006).

[40] Luschtinetz, R., Frenzel, J., Milek, T. & Seifert, G. *J. Phys. Chem. C* **113**, 5730 (2009).

[41] Nilsing, M., Persson, P., Lunell, S. & Ojamäe, L. Dye-Sensitization of the TiO_2 Rutile (110) Surface by Perylene Dyes: Quantum-Chemical Periodic B3LYP Computations. *J. Phys. Chem. C* **111**, 12116 (2007).

[42] Gundlach, L. *et al.* Different orientations of large rigid organic chromophores at the rutile TiO_2 surface controlled by different binding geometries of specific anchor groups. *Phys. Rev. B* **75**, 125320 (2007).

[43] Ziman, J. M. *Principles of the theory of solids*, 200–203 (Cambridge University Press, 1989), 2 edn.

APPENDIX A

BORN–OPPENHEIMER NONRELATIVISTIC APPROXIMATION

Born–Oppenheimer approximation simplifies the complicated many-body Hamiltonian considering the huge mass difference between electron and nucleus. Since the ratio m/M is smaller than $1/1000$, electron response to nuclear motion can be approximated as instantaneous. To see this one can make a clever guess describing the nuclei motion as simple harmonic oscillator, thus recommending the potential $V(R) = \frac{1}{2}M\omega^2R^2$. If a nucleus displaced from the equilibrium position by an amount of δ, change in potential is $\Delta V = \frac{1}{2}M\omega^2\delta^2$ then using Hellman–Feynman theorem 2.9, the force on the nucleus can be written as

$$f_R = \langle \psi_{ni}^{\text{nuc}} \mid \frac{1}{2}M\omega^2\delta^2 \mid \psi_{ni}^{\text{nuc}} \rangle \approx M.$$

Also disturbance in the nuclear position accounts for redistribution of electrons and again the force goes like M. The ratio of change in velocities of the nucleus and the electron is approximately $\delta v_e/\delta v_n \approx 10^3$. Therefore as far as electrons are concerned motion of nuclei is negligible. In other words, solution to Schrödinger equation with many-body Hamiltonian can be separated into nuclear and electronic wave functions. This is shown by Born and Oppenheimer [10] by expanding the energy in terms of the fourth root of mass ratio $(m/M)^{1/4}$ where nuclear vibrations are second order $(m/M)^{1/2}$ which is around 10^{-2}.

The approximation starts with the assumption that expands many body wave function in terms of the solutions of electronic Hamiltonian but the coefficients as the nuclei wave functions

$$\psi_n^{\text{tot}}(\mathbf{r}, \mathbf{R}) = \sum_{i=1}^{\infty} \psi_{ni}^{\text{nuc}}(\mathbf{R})\psi_i^{\text{el}}(\mathbf{r}, \mathbf{R}) \tag{A.1}$$

with

$$H_e\psi_i^{\text{el}}(\mathbf{r}, \mathbf{R}) = E_i^{\text{el}}(\mathbf{R})\psi_i^{\text{el}}(\mathbf{r}, \mathbf{R})$$

and

$$\int \psi_i^{\mathrm{el}^*}(\mathbf{r},\mathbf{R})\psi_j^{\mathrm{el}}(\mathbf{r},\mathbf{R})d\mathbf{r} = \delta_{ij}$$

where $\mathbf{r}$ shows electronic and $\mathbf{R}$ shows nuclear set of coordinates $\{\mathbf{r}_i\}$, $\{\mathbf{R}_k\}$. In addition $\psi_i^{\mathrm{el}}(\mathbf{r},\mathbf{R})$ is the solution to the Schrödinger equation for the electrons in a frozen lattice as R denoting the postions of static nuclei. Applying the many body Hamiltonian (2.1)[1]

$$H\psi_n^{\mathrm{tot}}(\mathbf{r},\mathbf{R}) = \sum_i^{\infty} T_n\left(\psi_{ni}^{\mathrm{nuc}}(\mathbf{R})\psi_i^{\mathrm{el}}(\mathbf{r},\mathbf{R})\right) + \psi_{ni}^{\mathrm{nuc}}(\mathbf{R})E_i^{\mathrm{el}}\psi_i^{\mathrm{el}}(\mathbf{r},\mathbf{R}) = E_n^{\mathrm{tot}}\sum_{i=1}^{\infty}\psi_{ni}^{\mathrm{nuc}}(\mathbf{R})\psi_i^{\mathrm{el}}(\mathbf{r},\mathbf{R}). \tag{A.2}$$

For the kinetic energy operator[2]

$$\begin{aligned}\sum_i^{\infty} T_n\left(\psi_{ni}^{\mathrm{nuc}} + \psi_i^{\mathrm{el}}\right) &= -\sum_i^{\infty}\sum_{k=1}^{M}\frac{1}{2M_k}\left(\nabla_k^2\psi_{ni}^{\mathrm{nuc}}\psi_i^{\mathrm{el}} + \psi_{ni}^{\mathrm{nuc}}\nabla_k^2\psi_i^{\mathrm{el}} + 2\nabla_k\psi_{ni}^{\mathrm{nuc}}\nabla_k\psi_i^{\mathrm{el}}\right)\\ &= -\sum_i^{\infty}\psi_i^{\mathrm{el}}\sum_{k=1}^{M}\frac{1}{2M_k}\nabla_k^2\psi_{ni}^{\mathrm{nuc}} - \sum_i^{\infty}\sum_{k=1}^{M}\frac{1}{2M_k}\left(\psi_{ni}^{\mathrm{nuc}}\nabla_k^2\psi_i^{\mathrm{el}} + 2\nabla_k\psi_{ni}^{\mathrm{nuc}}\nabla_k\psi_i^{\mathrm{el}}\right).\end{aligned}$$

Substituting this into (A.2), multiplying with $\psi_j^{\mathrm{el}^*}$ and integrating over electronic coordinates gives

$$\left(T_n + E_j^{\mathrm{el}}\right)\psi_{nj}^{\mathrm{nuc}} - \sum_{i=1}^{\infty}\sum_{k=1}^{M}\frac{1}{2M_k}\left(\psi_{ni}^{\mathrm{nuc}}\langle\psi_j^{\mathrm{el}} \mid \nabla_k^2 \mid \psi_i^{\mathrm{el}}\rangle + 2\nabla_k\psi_{ni}^{\mathrm{nuc}}\langle\psi_j^{\mathrm{el}} \mid \nabla_k \mid \psi_i^{\mathrm{el}}\rangle\right).$$

Second term and the first term in the double sum are called first and second order non-adiabatic coupling elements and these terms are ignored in the frame of an approximation which is the adiabatic approximation [43]. It says that nuclei move slow enough so that the electrons are not excited due to these vibrational and rotational motions. In other words if electronic energy levels are discrite enough or there exists no states close in energy then the electronic wave function is invariant under nuclei motion. In order to show non-adiabatic terms add small contributions to the energy, consider the first order non-adiabatic term which contributes nothing to the energy, i. e.

$$\begin{aligned}\sum_{i=1}^{\infty}\sum_{k=1}^{M}2\nabla_k\psi_{ni}^{\mathrm{nuc}}\langle\psi_j^{\mathrm{el}} \mid \nabla_k \mid \psi_i^{\mathrm{el}}\rangle &= \sum_{i=1}^{\infty}\sum_{k=1}^{M}2\nabla_k\psi_{ni}^{\mathrm{nuc}}\int d\mathbf{r}\psi_j^{\mathrm{el}^*}\nabla_k\psi_i^{\mathrm{el}}\\ &= \sum_{i=1}^{\infty}\sum_{k=1}^{M}2\nabla_k\psi_{ni}^{\mathrm{nuc}}\nabla_k\int d\mathbf{r}\psi_j^{\mathrm{el}^*}\psi_i^{\mathrm{el}}\\ &= 0.\end{aligned} \tag{A.3}$$

[1] V_n is removed from Hamiltonian since it only contributes as a constant in the frame of initial assumption (for each case there is a defined set of nuclear position $\mathbf{R}$)

[2] Variables of the wave functions $\mathbf{R}$ and $\mathbf{r}$ are not written for convenience

The second order term is largest when the electrons are tightly bounded to their ions thus $\nabla_k \to \nabla_I$ where I is electronic set of coordinates, then

$$\sum_{i=1}^{\infty}\sum_{k=1}^{M}\frac{1}{2M_k}\psi_{ni}^{\text{nuc}}\langle\psi_j^{\text{el}} \mid \nabla_k^2 \mid \psi_i^{\text{el}}\rangle = \sum_{i=1}^{\infty}\sum_{k=1}^{M}\psi_{ni}^{\text{nuc}}\frac{1}{M_k}\int d\mathbf{r}\psi_j^{\text{el}}\frac{1}{2}\nabla_I^2\psi_i^{\text{el}}. \tag{A.4}$$

Last integral in above equation is just the kinetic energy of electrons multiplied with $1/M$ which is in atomic units and corresponds to ratio of electron and nuclear mass m/M in SI units. This ratio is of the order 10^{-3} to 10^{-4} and together with (A.3) it is clarified that ignorance of non-adiabatic terms does not change the results considerably.

Finaly returning to (A.2) and ignoring the non-adiabatic terms one can get the Schrödinger-type equation for the neclei inside a effective potential due to the electrons

$$\Big(T_n + E_i^{\text{el}}(\mathbf{R}) + V_n(\mathbf{R})\Big)\psi_{ni}^{\text{nuc}}(\mathbf{R}) = E_n^{\text{tot}}\psi_{ni}^{\text{nuc}}(\mathbf{R}). \tag{A.5}$$

For each set o nuclear positions the Schrödinger equation with electronic Hamiltonian has to be solved to get electronic ground state energy depending only on nuclei configuration and after that (A.5) can be solved to get minimum energy configuration.